Università degli Studi di Padova

Dipartimento di Fisica e Astronomia "Galileo Galilei"

Corso di Laurea Magistrale in
Fisica

Superconducting transport through a quantum dot with spin-orbit coupling

Relatore:
Dott. Luca Dell'Anna

Laureanda: Cliò Efthimia Agrapidis
Matricola: 1081527

Anno Accademico 2014/2015

If you try and take a cat apart to see how it works, the first thing you have on your hands is a nonworking cat.

D. Adams, `The Salmon of Doubt: Hitchhiking the Galaxy One Last Time`

ABSTRACT

Transport properties in mesoscopic systems are and have been of great scientific interest. In this work, we numerically analyze in detail the Josephson current in a double quantum dot with spin orbit coupling and an applied magnetic field in the limit of large $|\Delta|$, finding characteristic discontinuities in the current-phase relation and giving a possible explanation for their appearance. Furthermore, we put the basis for the numerical computation of the current in the non equilibrium case, making use of the Keldysh formalism.

Contents

1 Introduction

Transport properties in nanoscopic and mesoscopic systems have always attracted a lot of interest, for their potential applications, both from experimental and theoretical sides. The realization of perfectly tunable setups is a challenging task for the experimentalists, and, at the same time, an extraordinary playground for the theorists to benchmark their models and predictions. Nowadays nanotechnologies are improving faster and faster, not only in assempling always new nano-structures, but also in controlling and tuning the physical knobs of those novel devices. Hence, systems like superconductor-quantum dot-superconductor (S-QD-S) junction are more and more precisely characterized in their components. In these systems, quantum dots can be provided by semiconductor nanowires.

Recently it has been proved that a p-wave superconductor can be realized putting a quantum wire with strong spin-orbit interaction (InAs, InSb..) on top of a conventional s-wave superconductor (Nb, Ti, Tl) [1]. It has been shown [2, 3, 4] that in such system Majorana edge states should appear.

In this thesis we will focus our attention to a double level quantum dot with spin-orbit coupling in contact with two s-wave superconductors. A quantum dot is a physical structure small enough to exhibit quantum mechanical properties. It may have a number n of accessible levels. In the studied case, the quantum dot has two levels. This permits to include the spin-orbit interaction effects in our model. In a system composed by a quantum dot between two superconductors, it is expected to observe a current flowing even in the equilibrium conditions. This current is known as Josephson current.

The Josephson effect was predicted by B. D. Josephson in 1962 [5] and first observed by Anderson and Rowell in 1963 [6]. The original work by Josephson has been later extended by others (e.g. de Gennes in 1966 [7]) to include any type of "weak link" between the superconductors. From its first observation, this effect has been both theoretically and experimentally studied, leading to different development, e.g. in sensor for detecting ultralow magnetic field and weak electromagnetic radiation. The Josephson effect can be roughly described as the presence of a current occurring in the equilibrium state in systems of the form superconductor-material-superconductor. The material can be a normal conductor (SNS junction), an insulator (SIS junction), a double barries (SINIS junction), a ferromagnet (SFS junction), a two dimensional electron gas (S-2DEG-S junction) or a constriction (ScS junction). This current depends on the difference between the phases of the order parameters characterizing the two superconductors. This dependence is called current-phase relation (CPR or CϕR). The form of the flowing Josephson current in the weak contact limit is $I_J = I_c \sin(\phi)$. This phenomenon is strictly related to Andreev reflection, which are better treated in section 2.4. The Andreev reflections lead to the destruction of Cooper pairs allowing for electrons to pass through the impurity, bringing to the existence of the Josephson current.

In the following chapter of this thesis, we are going to describe the theory related to mesoscopic systems and superconductors, showing how the Josephson current can be computed and giving a brief description of Andreev reflections. Next, in the third chapter, we are focusing on a specific model of a double quantum dot with spin orbit coupling between superconducting leads in the equilibrium case, computing the Josephson current as the dot Hamiltonian parameters vary. In closing this chapter, we demonstrate how this model can be mapped into a Kitaev chain in a certain energy limit, thus connecting the discontinuity of the current to Majorana fermions signatures. In the fourth chapter, we study the same system out of equilibrium, finding a good form for the current to be numerically computed. Finally, we present the conclusion of our work.

2 The system

In this chapter, we are going to give an overview on the theory concerning the "ingredients" composing our system, that is a double quantum dot with spin-orbit coupling between superconducting leads. In particular, we are going to start from the definition of mesoscopic systems and quantum dots, then recall the BCS theory for superconductors. Moreover, we will explain the Josephson current phenomenon and, finally, we will introduce Andreev reflections.

2.1 Mesoscopic systems

The main characteristic of mesoscopic systems is that they are coherent, i.e. the quantum mechanical coherence length is longer than the sample size. This implies that all the phenomena regarding those systems are of quantum nature and shall be treat using the quantum formalism. As we are dealing with a coherence length, a good characterization of a mesoscopic system is possible via comparison of its typical lengths. Following H. Bruus and K. Flensberg [8], the important length scales are the coherence length ℓ_ϕ, the energy relaxation length, ℓ_{in}, the elastic mean free path, ℓ_0, the Fermi wave length of the electron, λ_F , the atomic Bohr radius, a_0, and of course the sample size, $\mathcal{L}$. A mesoscopic regime is then such that

$$a_0 \ll \lambda_F \leqslant \ell_0 < \mathcal{L} < \ell_\phi \leqslant \ell_{in} \tag{2.1}$$

Typical mesocopic systems are composed by quantum dots between some kind of leads (superconductors, metals). Specifically, those quantum dots are experimentally provided, for example, by semiconducting nanowires. A quantum dot can be think of as a confined atom whose orbital levels are "controlled" in the sense that they are not all accessible, i.e. just a fixed number n of levels is available for the electrons.

Quantum dots may also act as magnetic impurities. Thus, we also have evidence of Kondo effect is such systems. This effect describes an unusual scattering process of conduction electrons in a a metal with magnetic impurities. It was first predicted by J. Kondo in 1964 [9], who demonstrated how a contribution porportional to $\ln T$ is present at low temperature. Important contribution to its understanding were provided by P.W. Anderson with his Anderson impurity model and the accompanying renormalization theory [10] . We are not entering into the details of the calculation, but we report that this scattering process requires a spin-flip in the impurity. The possibility to observe this phenomenon in quantum dot junctions was theoretically proposed by Glazman and Raikh, Ng and Lee, both in 1988 [11, 12]. For this effect to be seen in quantum dot, it is necessary that at least one unpaired electron behaves ad a magnetic impurity, i.e. a quantum dot surely undergoes Kondo effect if it has an odd number of electron in it. However, this is not the only required condition, in fact, we are at temperature well below the Kondo temperature T_K, and hence the unpaired electron is more probably in a state far under the Fermi

level, while there is an empty state above this level. This implies that there is a terribly small probability for an electron to enter the dot from the leads: this is known as the Coulomb blockade regime. Nonetheless, at very low temperatures when a Kondo resonance develops at the Fermi level, arising from the interaction of the unpaired dot electron with the electrons in the lead and reservoirs, the states in the resonance allow the electron to pass through freely, the first observation of such a phenomenon was made in 1998 [13]. More experimental results linked to this effect in quantum dots can be found, e.g., in references [14, 15, 16].

This peculiar systems have a distinct behavior which we will underline in the next sections.

2.2 Superconducting leads

Superconductivity was first observed by H. K. Onnes in 1911. He noticed that really pure samples of different metals showed a dropping in the resistance while the temperature decreased. Moreover, the critical temperature T_c at which the dropping occurred depended on the material. As the resistance is the inverse of the conductance, he called this phenomenon superconductivity. Besides the zero-resistivity, superconductors have important magnetic characteristics, like the Meissner effect, consisting of the ejection of the magnetic field lines from the interior of the superconductor.

After those experimental discoveries, it was proposed, in 1935 [**?**], a phenomenological model, known as London theory, that could well reproduce the observation, but was not able to give a microscopic explanation to the phenomenon.

The microscopic theory was introduced in 1957 and it is noted as BCS theory by the initial of Bardeen, Copper and Schrieffer citeBCS1, BCS2. We can summarize their work as follows:

1. There exists an effectively attractive interaction between the electrons (due to the electron-phonon coupling)

2. Two electrons above the Fermi sea plus an attractive interactions give rise to a coupled state (known as Cooper pairs)

3. The ground state is a coherent state made of Cooper pairs

The action for the BCS model reads:

$$S = \int d\mathbf{r} \int d\tau \left[\sum_{\sigma} \left(\overline{\psi}_{\sigma}(\mathbf{r},\tau)(\partial_{\tau} - \frac{\nabla^2}{2m} - \mu)\psi_{\sigma}(\mathbf{r},\tau) \right) - g\,\overline{\psi}_{\uparrow}(\mathbf{r},\tau)\overline{\psi}_{\downarrow}(\mathbf{r},\tau)\psi_{\downarrow}(\mathbf{r},\tau)\psi_{\uparrow}(\mathbf{r},\tau) \right] \tag{2.2}$$

We now need to decouple the two-bodies interaction term. From the point of view related to the Hubbard-Stratonovich transformation we are performing, there are no differences in separating the interaction term via an operator related to the density or via an operator related to the Cooper pairs. However, those two channels

are physically different, and it is important to enucleate the one that is better from an energetic point of view. We then write

$$e^{\int g\overline{\psi}_\uparrow\overline{\psi}_\downarrow\psi_\downarrow\psi_\uparrow} = \int \mathcal{D}(\Delta^*\Delta)e^{-\int\frac{|\Delta^2|}{g}-(\Delta^*\psi_\downarrow\psi_\uparrow+\Delta\overline{\psi}_\uparrow\overline{\psi}_\downarrow)} \tag{2.3}$$

We now introduce the Nambu space, which has a 2×2 structure. We start defining the Nambu spinors

$$\mathbf{\Psi} = \begin{pmatrix}\psi_\uparrow\\ \overline{\psi}_\downarrow\end{pmatrix} \qquad \mathbf{\Psi}^\dagger = (\overline{\psi}_\uparrow \quad \psi_\downarrow) \tag{2.4}$$

Thus, we can write the partition function

$$Z = \int(\mathbf{\Psi}^\dagger\mathbf{\Psi})\int\mathcal{D}(\Delta^*\Delta)e^{-\int\frac{|\Delta|^2}{g}-\mathbf{\Psi}^\dagger G^{-1}\mathbf{\Psi}} \tag{2.5}$$

And the propagator G^{-1} is a 2×2 matrix in Nambu space

$$G^{-1} = \begin{pmatrix}-\partial_\tau+\frac{\nabla^2}{2m}+\mu & \Delta\\ \Delta^* & -\partial_\tau-\frac{\nabla^2}{2m}-\mu\end{pmatrix} \tag{2.6}$$

Exploiting the Gaussian form of the integration in $\mathbf{\Psi}^\dagger$, $\mathbf{\Psi}$, we have

$$Z = \int\mathcal{D}(\Delta^*\Delta)e^{-\int\frac{|\Delta|^2}{g}-\ln[G^{-1}]} \tag{2.7}$$

In the saddle-point approximation, and with the additional assumption that the minimizing Δ is homogeneous, we find the gap equation:

$$\frac{1}{g} = \nu_0\int_0^{\omega_D} d\xi\frac{\tanh\left(\frac{\sqrt{\xi^2+|\Delta|^2}}{2T}\right)}{\sqrt{\xi^2+|\Delta|^2}} \tag{2.8}$$

$$|\Delta| = 2\hbar\omega_D e^{-\frac{1}{g\nu_0}} \qquad \text{at } T=0 \tag{2.9}$$

Where ω_D is the Debye frequency and ν_0 is the density of states in the Fermi level. We remark that this form for Δ is valid for $T=0$. In general, Δ will depend on the temperature and, given that it is related to the Cooper pairs coupling energy, we can assert $|\Delta|$ is the superconducting order parameter.

To see the temperature dependence of our order parameter, we suppose temperature fluctuations to decrease the $|\Delta|$ value and that there exist a critical value $T=T_c$ such that $|\Delta|=0$. From the gap equation, we get $T_c = \gamma/\pi 2\omega_d e^{-\frac{1}{g\nu_0}}$. Employing Ginzburg-Landau theory for phase transitions, we expand the action near T_c until fourth order in $|\Delta|$ (note that all the odd contribution to the term $\mathrm{Tr}\ln G^{-1}$ vanishes) and find that the transition is of the second order: for $T<T_c$ we have two minima that, while T increases versus T_c, shift until they both reach the local maximum, vanishing.

We conclude this excursus in superconductivity theory inserting an external electromagnetic field in the system via minimal substitution.Writing the gap in the

form $\Delta = \Delta_0 e^{2i\theta}$, it is easy to see that the BCS model is not invariant for $U(1)$ transformation. We can get rid of the gap phase via a unitary trnsformation

$$U = \begin{pmatrix} e^{-i\theta} & 0 \\ 0 & e^{i\theta} \end{pmatrix}$$

In this way, if the phase fluctuates in time-space, we will have additional terms on the diagonal of G^{-1}. Expanding for small electromagnetic field and small phase fluctuation, then taking the field to be null, we write the Goldstone action for superconductors

$$S[\theta] = \int d\tau \int d\mathbf{r} \left[c_1 (\partial_\tau \theta)^2 + c_2 (\nabla \theta)^2 \right] \tag{2.10}$$

with $c_1 \propto \nu$ and $c_2 \propto n_s/2m$, where n_s is the Cooper pairs density.

2.3 Josephson current

The Josephson current is a macroscopic quantum phenomenon that occurs at a junction between two superconductors and consists of a supercurrent, i.e. a dissipationless current at equilibrium, flowing between the two superconductors. Denoting with N_j the electron number operator in the $j = L, R$ lead, we have

$$\langle I_L \rangle = \langle \dot{N}_L \rangle = i[H, N_L]$$
$$\langle I_R \rangle = \langle \dot{N}_R \rangle = i[H, N_R]$$

The J-current is the half net current

$$I = \frac{\langle I_L \rangle - \langle I_R \rangle}{2} \tag{2.11}$$

The Hamiltonian H is necessarily composed of the superconductors contribution and of a tunelling Hamiltonian describing the tunneling effect within the superconductors and the junction. As we are dealing with a superconductor-quantum dot-superconductor system, we will also include the dot Hamiltonian. Thus

$$H = H_0 + H_{dot} + H_t$$

Where H_0 describes the superconductors, H_{dot} is the dot Hamiltonian and H_t is the tunneling one. They respectively read

$$H_0 = \int \frac{d^3k}{(2\pi)^3} \sum_{\sigma,j} [\epsilon(\mathbf{k}) - \mu_j] c^\dagger_{\sigma,j}(\mathbf{k}) c_{\sigma,j}(\mathbf{k}) - \int \frac{d^3k}{(2\pi)^3} \sum_j \left(\Delta_j c^\dagger_{\uparrow,j}(\mathbf{k}) c^\dagger_{\downarrow,j}(-\mathbf{k}) + \text{h.c.} \right) \tag{2.12a}$$

$$H_t = - \int \frac{d^3k}{(2\pi)^3} \sum_{\sigma,j} \left(t_j c_{\sigma,p}(\mathbf{k}) d^\dagger_\sigma + \text{h.c.} \right) \tag{2.12b}$$

$$H_{dot} = \epsilon_0 (n_\uparrow + n_\downarrow) - \frac{U}{2} (n_\uparrow - n_\downarrow)^2 \tag{2.12c}$$

The last equation, derives from an Anderson-type Hamiltonian. Using $\epsilon_0 = E_0 + U/2$ and $n_\sigma^2 = n_\sigma = d_\sigma^\dagger d_\sigma = 0, 1$, we get

$$\begin{aligned} H_{\text{dot}} &= E_0 \sum_\sigma n_\sigma + U n_\uparrow n_\downarrow \\ &= E_0(n_\uparrow + n_\downarrow) + \frac{U}{2}(n_\uparrow + n_\downarrow) - \frac{U}{2}(n_\uparrow + n_\downarrow) + U n_\uparrow n_\downarrow \\ &= \epsilon_0(n_\uparrow + n_\downarrow) - \frac{U}{2}(n_\uparrow - n_\downarrow)^2 \end{aligned}$$

We assume the tunnel couplings $t_{L/R}$ to the dot to be real and $\mathbf{k}$-independent for simplicity.

Let us first consider the equilibrium problem ($\mu_L = \mu_R$), i.e. work in Euclidean time. With fermion Matsubara frequencies $\omega_n = (2n+1)\pi/\beta$ and Grassmann fields ψ, $\overline{\psi}$ corresponding to the operators $c_{\sigma,p}(\mathbf{k},\tau)$, $c^\dagger(\mathbf{k},\tau)$:

$$\psi_{\sigma,p}(\mathbf{k},\tau) = \frac{1}{\beta}\sum_{\omega_n} e^{-i\omega_n\tau}\psi_{\sigma,p}(\mathbf{k},\omega_n) \tag{2.13a}$$

$$\overline{\psi}_\sigma, p(\mathbf{k},\tau) = \frac{1}{\beta}\sum_{\omega_n} e^{i\omega_n\tau}\overline{\psi}_{\sigma,p}(\mathbf{k},\omega_n) \tag{2.13b}$$

we can form Nambu 2-spinors, as seen in section 2.2. We will use the abbreviation

$$\sum{}' = \frac{1}{\beta}\sum_{\omega_n}\int\frac{d^3k}{(2\pi)^3}$$

The Euclidean action S_0 describing H_0 is the usual superconducting action

$$S_0 = -\sum_j \sum{}' \mathbf{\Psi}_j^\dagger(\mathbf{k},\omega_n) G_j^{-1}(\mathbf{k},\omega_n)\mathbf{\Psi}_j(\mathbf{k},\omega_n) \tag{2.14}$$

with

$$G_j^{-1}(\mathbf{k},\omega_n) = \begin{pmatrix} i\omega_n - \epsilon_k & \Delta_j \\ \overline{\Delta}_j & i\omega_n + \epsilon_k \end{pmatrix} \tag{2.15}$$

To incude μ_j, let $\epsilon_k \to \epsilon_k - \mu_j$. Computing the inverse we have

$$G_j(\mathbf{k},\omega_n) = \frac{1}{\omega_n^2 + \epsilon_k^2 + |\Delta_j|^2}\begin{pmatrix} -i\omega_n - \epsilon_k & \Delta_j \\ \overline{\Delta}_j & -i\omega_n \epsilon_k \end{pmatrix} \tag{2.16}$$

We also define the bispinors for the Grassmann fields of the dot

$$\mathbf{D}(\tau) = \begin{pmatrix} d_\uparrow(\tau) \\ \overline{d}_\downarrow(\tau) \end{pmatrix} = \frac{1}{\beta}\sum_{\omega_n} e^{-i\omega_n\tau}\mathbf{D}(\omega_n) \qquad \mathbf{D}(\omega_n) = \begin{pmatrix} d_\uparrow(\omega_n) \\ \overline{d}_\downarrow(-\omega_n) \end{pmatrix}$$

Note that

$$\mathbf{D}^\dagger\mathbf{D} = \begin{pmatrix} \overline{d}_\uparrow & d_\downarrow \end{pmatrix}\begin{pmatrix} d_\uparrow \\ \overline{d}_\downarrow \end{pmatrix} = \overline{d}_\uparrow d_\downarrow + d_\downarrow \overline{d}_\downarrow = n_\uparrow - n_\downarrow \tag{2.17}$$

While, denoting the Pauli matrix acting on the Nambu space with τ_i

$$\mathbf{D}^\dagger\tau_3\mathbf{D} = \begin{pmatrix} \overline{d}_\uparrow & d_\downarrow \end{pmatrix}\begin{pmatrix} 1 & 0 \\ 0 & -1 \end{pmatrix}\begin{pmatrix} d_\uparrow \\ \overline{d}_\downarrow \end{pmatrix} = n_\uparrow + n_\downarrow \tag{2.18}$$

Using (2.17) and (2.18) we can write, for the dot action

$$S_{dot} = \int d\tau \left(\mathbf{D}^\dagger(\tau)(\partial_\tau \tau_0 + \epsilon_0 \tau_3)\mathbf{D}(\tau) - \frac{U}{2}(\mathbf{D}^\dagger \mathbf{D})^2 \right) \tag{2.19}$$

The coupling between leads and dot gives the action

$$S_I = \sum_j t_j {\sum}' \left(\mathbf{D}^\dagger(\omega_n)\tau_3 \mathbf{\Psi}_j(\mathbf{k}, \omega_n) + \mathbf{\Psi}_j^\dagger(\mathbf{k}, \omega_n)\tau_3 \mathbf{D}(\omega_n) \right) \tag{2.20}$$

as can be seen via direct calculation.

We are interested in the current through the dot. We are still working in the equilibrium case, so there is no applied voltage ($V = 0$). The current through the left/right contact oriented towards the dot is:

$$I_{j=L/R} = e \left\langle \frac{d}{dt} \sum_{\mathbf{k},\sigma} n_{\sigma,j}(\mathbf{k}) \right\rangle = e \left\langle \frac{d}{dt} \sum_{\mathbf{k},\sigma} c^\dagger_{\sigma,j}(\mathbf{k}) c_{\sigma,j}(\mathbf{k}) \right\rangle \tag{2.21}$$

$$= e \left\langle \sum_{\mathbf{k},\sigma} \left[\frac{d}{dt} c^\dagger_{\sigma,j}(\mathbf{k}) \right] c_{\sigma,j}(\mathbf{k}) + \sum_{\mathbf{k},\sigma} c^\dagger_{\sigma,j}(\mathbf{k}) \left[\frac{d}{dt} c_{\sigma,j}(\mathbf{k}) \right] \right\rangle \tag{2.22}$$

Computing the commutators and averaging over imaginary time gives ($j = +1$ for $j = L$, $j = -1$ for $j = R$).

$$I = -\frac{ie}{2\hbar\beta} {\sum}' \sum_j j t_j \left\langle \left[\mathbf{\Psi}_j^\dagger \mathbf{D} - \mathbf{D}^\dagger \mathbf{\Psi}_j \right] \right\rangle \tag{2.23}$$

t is to be noted that the elements of the form $c^\dagger_\uparrow c^\dagger_\downarrow$ from the commutators with H_0 remaining in the $\sum_\sigma$ are of the form $\sim \Delta^*$ when we consider the expectation value, so they cancel out between themselves.
To extract the Josephson current I, in the equilibrium case, we can add a source term to the total action:

$$S_J = -\frac{iew}{2\beta\hbar} \sum_j j t_j {\sum}' \left(\mathbf{D}^\dagger \mathbf{\Psi}_j - \mathbf{\Psi}_j^\dagger \mathbf{D} \right) \tag{2.24}$$

Thus, the partition function is

$$Z(w) = \int \mathcal{D}[\mathbf{\Psi}^\dagger \mathbf{\Psi}] \int \mathcal{D}[\mathbf{D}^\dagger \mathbf{D}] \exp[-(S_0 + S_I + S_{dot} + S_J)] \tag{2.25}$$

and we can write the current as

$$I_J = \frac{d}{dw} \ln Z(w = 0) = \frac{1}{Z(w = 0)} \frac{d}{dw} Z(w = 0) \tag{2.26}$$

Introducing new Grassman auxiliary bispinors $\mathbf{K}, \mathbf{K}^\dagger$, we can integrate the Nambu spinors and find an effective dot action. We define

$$\mathbf{K}(\tau) = \left(\tau_3 \pm \frac{iewp}{2\beta} \tau_0 \right) \mathbf{D}(\tau) \tag{2.27}$$

Thus

$$\exp\left[-\int_0^\beta d\tau \int \frac{d\mathbf{k}}{(2\pi)^3}\left(\mathbf{\Psi}^\dagger G^{-1}\mathbf{\Psi} + \mathbf{D}^\dagger(\partial_\tau\tau_0 + \epsilon_0\tau_3)\mathbf{D} - \frac{U}{2}(\mathbf{D}^\dagger\mathbf{D})^2 + t_j(\mathbf{d}^\dagger\tau_3\mathbf{\Psi} + \mathbf{\Psi}^\dagger\tau_3\mathbf{D})\right.\right.$$
$$\left.\left. -\frac{iew}{2\beta\hbar}pt_j(\mathbf{D}^\dagger\mathbf{\Psi} - \mathbf{\Psi}^\dagger\mathbf{D})\right)\right] \to \exp\left[-\sum_j{\sum}'\left(\mathbf{\Psi}_j^\dagger(-G_j)^{-1}\mathbf{\Psi}_j + t_j(\mathbf{K}\mathbf{\Psi}_j + \mathbf{\Psi}_j^\dagger\mathbf{K})\right)\right] \tag{2.28}$$

Now we have a quadratic form in $\mathbf{\Psi}$, so we can use the generalized Gaussian integration and write, for the effective action S_{env} (the prefactor is put into the normalization)

$$e^{-S_{env}} = \int \mathcal{D}[\mathbf{\Psi}^\dagger\mathbf{\Psi}]\exp\left[-\sum_j{\sum}'\left(\mathbf{\Psi}_j^\dagger(-G_j)^{-1}\mathbf{\Psi}_j + t_j(\mathbf{K}\mathbf{\Psi}_j + \mathbf{\Psi}_j^\dagger\mathbf{K})\right)\right] =$$
$$= \exp\left[-\sum_j t_j^2{\sum}'\mathbf{K}^\dagger G_j\mathbf{K}\right]$$

And we found

$$S_{env} = \frac{1}{\beta}\sum_{\omega_n}\mathbf{K}^\dagger(\omega_n)\widetilde{\Sigma}(\omega_n)\mathbf{K}(\omega_n) \tag{2.29}$$

with

$$\widetilde{\Sigma}(\omega_n) = \sum_j t_j^2\int\frac{d^3k}{(2\pi)^3}G_j(\mathbf{k},\omega_n) \tag{2.30}$$

and this is a matrix in Nambu space. We define a 3D density of states and we assume it is identical on both sides

$$N_0 = \frac{k_F^2}{2\pi^2 v_f} \tag{2.31}$$

We also define hybridization matrix elements

$$\Gamma_j = \pi N_0 t_j^2 \tag{2.32}$$

We re-absorbe μ_j in ϵ_k and, once computed the angular integrals, we have

$$\begin{aligned}\widetilde{\Sigma}(\omega_n) = &\sum_j t_j^2\int_0^{+\infty}\frac{k^2dk}{2\pi^2}\frac{1}{\omega_n^2+\epsilon_k^2+|\Delta|^2}\begin{pmatrix}-i\omega_n-\epsilon_k & \Delta_j\\ \overline{\Delta}_j & -i\omega_n+\epsilon_k\end{pmatrix}\\ \simeq &\sum_j t_j^2 N_0\int_{-\infty}^{\infty}d\epsilon\frac{1}{\omega_n^2+\epsilon^2+|\Delta|^2}\begin{pmatrix}-i\omega_n-\epsilon & \Delta_j\\ \overline{\Delta}_j & -i\omega_n+\epsilon\end{pmatrix}\end{aligned} \tag{2.33}$$

When we integrate, the terms linear in ϵ vanish. We continue defining the self-energy

$$\Sigma(\omega_n) = \tau_3\widetilde{\Sigma}(\omega_n)\tau_3 = -\sum_j\frac{\Gamma_j}{\pi}\int_0^{+\infty}\frac{d\epsilon}{\omega_n^2+\epsilon^2+|\Delta_j^2|}\begin{pmatrix}i\omega_n & \Delta_j\\ \overline{\Delta}_j & i\omega_n\end{pmatrix} \tag{2.34}$$

We now split the effective action into different components.
The w independent term is

$$S_{env}(w=0) = \frac{1}{\beta}\sum_{\omega_n} \mathbf{D}^\dagger(\omega_n)\Sigma(\omega_n)\mathbf{D}(\omega_n) \tag{2.35}$$

For the Josephson current, we need the terms linear in w. We call this contribution S'_{env} and is such that the complete term is given by wS'_{env}

$$\begin{aligned} S'_{env} &= \frac{1}{\beta}\sum_{\omega_n} \frac{ie}{2\beta} j \left(\mathbf{D}^\dagger \tau_3 \widetilde{\Sigma}\mathbf{D} - \mathbf{D}^\dagger \widetilde{\Sigma}\tau_3 \mathbf{D}\right) \\ &= -\frac{ie}{2\beta}\frac{1}{\beta}\sum_{\omega_n} p\mathbf{D}^\dagger \left[\widetilde{\Sigma}, \tau_3\right]\mathbf{D} \end{aligned} \tag{2.36}$$

We denominate the Josephson self-energy

$$\begin{aligned} \Sigma^J(\omega_n) &= \frac{-iej}{2\beta}\left[\widetilde{\Sigma}, \tau_3\right] \\ &= \sum_j \frac{ie\Gamma_j}{2\beta\pi} j \int_0^{+\infty} p\int \frac{d\epsilon}{\omega_n^2 + |\Delta_j|^2 + \epsilon^2}\left[\begin{pmatrix} -i\omega_n & \Delta_j \\ -\overline{\Delta}_j & i\omega_n \end{pmatrix} - \begin{pmatrix} -i\omega_n & -\Delta_j \\ \overline{\Delta}_j & i\omega_n \end{pmatrix}\right] \\ &= \sum_j \frac{ie\Gamma_j}{\beta\pi} j \int \frac{d\epsilon}{\omega_n^2 + |\Delta_j|^2 + \epsilon^2}\begin{pmatrix} 0 & \Delta_j \\ -\overline{\Delta}_j & 0 \end{pmatrix} \end{aligned} \tag{2.37}$$

And we conclude

$$S'_{env} = \frac{1}{\beta}\sum_{\omega_n} \mathbf{D}^\dagger \Sigma^J(\omega_n)\mathbf{D}(\omega_n) \tag{2.38}$$

Therefore the elimination of the leads cost us the introduction of a self-energy for the dot. We can now integrate in $d\epsilon$ with $\int d\epsilon \left(E^2 + \epsilon^2\right)^{-1} = \pi/|E|$.

$$\Sigma(\omega_n) = -\sum_j \frac{\Gamma_j}{\sqrt{\omega_n^2 + |\Delta_j|^2}}\begin{pmatrix} i\omega_n & \Delta_j \\ \overline{\Delta}_j & i\omega_n \end{pmatrix} \tag{2.39a}$$

$$\Sigma^J(\omega_n) = \sum_j \frac{ie\Gamma_j}{\beta} j \frac{1}{\sqrt{\omega_n^2 + |\Delta_j|^2}}\begin{pmatrix} 0 & \Delta_j \\ -\overline{\Delta}_j & 0 \end{pmatrix} \tag{2.39b}$$

In a symmetric situation we have $|\Delta_j| = \Delta$, $\Gamma_j = \Gamma/2$ and $\phi_L = -\phi_R = \phi/2$. Then

$$\begin{aligned} \Sigma(\omega_n) &= -\frac{\Gamma}{2\sqrt{\omega_n + \Delta^2}}\left[\begin{pmatrix} i\omega_n & \Delta e^{\frac{i\phi}{2}} \\ \Delta e^{-\frac{i\phi}{2}} & i\omega_n \end{pmatrix} + \begin{pmatrix} i\omega_n & \Delta e^{-\frac{i\phi}{2}} \\ \Delta e^{\frac{i\phi}{2}} & i\omega_n \end{pmatrix}\right] \\ &= -\frac{\Gamma}{2\sqrt{\omega_n + \Delta^2}}\begin{pmatrix} 2i\omega_n & \Delta(e^{\frac{i\phi}{2}} + e^{-\frac{i\phi}{2}}) \\ \Delta(e^{-\frac{i\phi}{2}} + e^{\frac{i\phi}{2}}) & 2i\omega_n \end{pmatrix} \\ &= -\frac{\Gamma}{\sqrt{\omega_n + \Delta^2}}\begin{pmatrix} 2i\omega_n & \Delta\cos(\phi/2) \\ \Delta\cos(\phi/2) & i\omega_n \end{pmatrix} \\ &= -\frac{\Gamma}{\sqrt{\omega_n + \Delta^2}}\left(i\omega_n\tau_0 + \Delta\cos(\phi/2)\tau_1\right) \end{aligned} \tag{2.40}$$

and similarly we find

$$\Sigma^J(\omega_n) = -\frac{e\Gamma\Delta\sin(\phi/2)}{\hbar\beta\sqrt{\Delta^2 + \omega_n^2}}\tau_1 \tag{2.41}$$

2.4 Andreev reflections

We close this first chapter with a brief review on Andreev reflections.

We consider a superconductor-normal conductor-superconductor (SNS) junction. At the NS interface, the electrical current is partially converted into supercurrent, the conversion depending on the nature of the interface.

If we have a high-barrier tunneling junction the fraction of the current delivered to the supercurrent as a nonequilibrium charge can be computed considering the charge of each quasiparticle injected and the injection rate. For $T \approx 0$ and an applied bias $eV = \Delta$, the quasiparticle is created by injecting an electron right in the gap edge $E_k = \Delta$. This leads to a null contribution to the nonequilibrium charge, as those states are a mixture of hole and electrons and, thus, have zero charge. If the bias (or the temperature) is higher, the transmitted charge is nonzero and it tends to unity for $E_k \gg \Delta$.

In the opposite limit, we have what is known as Andreev reflections. For electron with $E \gg \Delta$, we recover what said above. The major effect is given by electrons with $E < \Delta$: when the interface is reached, they cannot enter the superconductor as quasiparticles because there are no quasiparticles states in the gap and they are reflected back in the normal conductor as holes, leading to a transferred charge of $2e$ across the interface. In the limit of kT and $eV \ll \Delta$, all electrons are Andreev reflected and this implies a differential conductance value twice that in the normal state.

Normally, a real junction will be in a state enclosed between this two limits. In a 1982 classic work, Klapwijk et al. [17, 18] presented what is now called the BTK model for multiple Andreev reflections. They studied different kind of barriers at the NS interface from the metallic limit to the tunnel junction and computed a family of $I - V$ curves. Let us consider an electron incidenting into the left lead after being accelerated by the eV bias: it undergoes an Andreev reflection and it is reflected back as a hole in the metallic link. As the charge of the particle is now opposite to the initial one, this is accelerated to the right lead and then Andreev reflected, this time as an electron. The transferred charge is always $2e$. Actual computation for the $I - V$ dependence have to take into account all the possible trajectories and use a Boltzmann equation approach if considering a barrier at the interface.

3 Equilibrium case

In this chapter, we are going to introduce the Hamiltonian of the system and study the current behavior in the equilibrium case, while varying the parameters regulating the dot Hamiltonian. In our calculations, we are taking $e = \hbar = k_b = 1$.

3.1 The system's Hamiltonian

The Hamiltonian is composed by three different contribution

$$H = H_d + H_t + H_l \tag{3.1}$$

Where H_d is the dot Hamiltonian, H_t the tunneling Hamiltonian and H_l the superconducting leads Hamiltonian. The characterizing property of the considered system is the spin-orbit interaction in the quantum-dot. The spin-orbit coupling is a quantum effect due to the interaction between the particle's spin and its motion. At the atomic level, it is observed as a splitting of the spectral lines and we can modeled it as a term proportional to $\mathbf{L} \cdot \mathbf{S}$. In condensed matter physics, the most striking observation of this interaction is the Rashba effect discovered in 1959 and sometimes referred to as Rashba-Dresselhaus effect, which is seen in two-dimensional systems. In particular, the Rashba effect is a momentum-dependent splitting of the spin bands in two-dimensional semiconducting heterostructures, generated by a combination of atomic spin-orbit coupling and the asymmetry of the confining potential in the direction perpendicular to the plane. Dresselhaus spin-orbit coupling, instead, is generated by the asymmetry in the bulk. This interaction can be written as

$$V_{SO} = \frac{\alpha_R}{\hbar}(\sigma_x p_y - \sigma_y p_x) + \frac{\alpha_D}{\hbar}(\sigma_x p_x - \sigma_y p_y) \tag{3.2}$$

Where α_R, α_D are the coupling strength of the Rashba and the Dresselhaus effect respectively.

In our model, we are going to consider a Rashba type spin-orbit interaction in the quantum dot. It is to be noted that a double quantum dot is the minimal working assumption for the spin-orbit coupling to be effective. Indeed, in a simple quantum dot this effect would not provide changes in the system Hamiltonian, as no spin-flip would be present.

As seen above, H_l can be written as

$$H_l = \sum_{j=L,R} \sum_{\mathbf{k}} \Psi^\dagger_{j\mathbf{k}} \begin{pmatrix} \xi_{\mathbf{k}} & \Delta_j \\ \Delta_j & -\xi_{\mathbf{k}} \end{pmatrix} \Psi_{j\mathbf{k}} \tag{3.3}$$

We are going to assume $\Delta_L = \Delta_R \equiv \Delta$ and $\Delta \geqslant 0$ real-valued, as its phase is guaged away from here and included into H_t.

We are neglecting the Coulomb interaction between electrons in the dot, thus we write

$$H_d = \sum_{n\sigma,n'\sigma'} d^\dagger_{n\sigma}\, h_{n\sigma,n'\sigma'}\, d_{n'\sigma'} \tag{3.4}$$

Where $d^\dagger_{n\sigma}$ creates a dot electron with spin σ with orbital quantum number n. h is a 4×4 Hermitian matrix that encapsulates the single-particle content. In particular:

$$h = (\mu\tau_0 + \epsilon\tau_z)\sigma_0 + B\tau_0\sigma_z + \alpha\tau_y[\cos(\chi)\sigma_z + \sin(\chi)\sigma_y] \tag{3.5}$$

And $\tau_{x,y,z}$ ($\sigma_{x,y,z}$) are Pauli matrices in orbital (spin) space, χ is a parameter related to the "angle" between the SOC and the Zeeman magnetic field B.

Finally, the tunneling Hamiltonian

$$H_t = \sum_{j=L,R}\sum_{\mathbf{k}}\sum_{n=1}^{2} \Psi^\dagger_{j\mathbf{k}} T_{j,n} D_n + \text{h.c.} \tag{3.6}$$

$$T_{j,n} = \begin{pmatrix} e^{i\phi_j/2}t_{j,n} & 0 \\ 0 & -e^{-i\phi_j/2}t^*_{j,n} \end{pmatrix}$$

Here ϕ_j is the superconducting phase of the j lead and we have introduced Nambu spinors for the dot: $D_n = (d_{n,\uparrow}, d^\dagger_{n,\downarrow})^T$.

We have already seen in sec. 2.3 how the Josephson current flows across the dot between the leads and that it follows, from the ground-state average,

$$I_j = \frac{2e}{\hbar}\partial_{\phi_j} F \tag{3.7}$$

With $F = -T\ln Z$ the free energy and Z has the form

$$Z = Z_l \mathrm{Tr}_d(e^{-\beta H_d}\, T\, e^{-S_t})$$

Where Tr_d is the trace over the dot Hilbert space and we have denoted with T the time-ordering operator, with Z_l the partition function of the leads and with S_t the tunneling action. From Wick's theorem, it follows that

$$S_t = -\frac{1}{2}\int_0^\beta d\tau d\tau' \langle T H_t(\tau) H_t(\tau')\rangle_l$$

Inserting H_t

$$S_t = \frac{1}{2}\int_0^\beta d\tau d\tau' \sum_{nn'} D^\dagger_n(\tau)\Sigma_{nn'}(\tau-\tau')D_{n'}(\tau')$$

Where

$$\Sigma_{nn'}(\tau-\tau') = 2\sum_j T^\dagger_{j,n} G_l(\tau-\tau') T_{j,n'}$$

Here, G_l is the superconducting Green function of the j lead and it is calculated from (2.6). Thus,

$$\Sigma_{nn'}(\tau) = \sum_{j=L,R}\Gamma^{(j)}_{n,n'}\begin{pmatrix} \partial_\tau & \Delta e^{-i\phi_j} \\ \Delta e^{i\phi_j} & \partial_\tau \end{pmatrix} f(\tau)$$

with $f(\tau) = T\sum_m \frac{e^{-i\omega_m\tau}}{\sqrt{\omega_m^2-\Delta^2}}$, and m is the label in the Matsubara frequency space $\omega_m = \pi T(2m+1)$. The 2×2 Hermitian matrix $\Gamma^{(j)}_{nn'} = 2\pi\nu_0 t^*_{j,n} t_{j,n'}$ describes the tunnel contacts and can be modeled as

$$\Gamma^{(j)} = \gamma_j \begin{pmatrix} e^{\lambda_j} & e^{i\delta_j} \\ e^{-i\delta_j} & e^{-\lambda_j} \end{pmatrix} \tag{3.8}$$

where $\gamma_j \geqslant 0$ gives the overall hybridization strength of the respective contact, λ_j parametrizes the orbital asymmetry and δ_j is an inter-orbital phase shift. We remark that, since δ_j is independent of spin, it has nothing to do with the SOC. For later purposes, we define the relative inter-orbital phase shift as

$$\delta = \delta_L - \delta_R \tag{3.9}$$

3.1.1 Superconducting atomic limit

We restrain our study to the specific case where Δ represents the biggest energy scale in the system. Formally, this is achieved taking the limit $\Delta \to \infty$. In this limit, $f(\tau) \to \Delta^{-1}\delta(\tau)$ and the partition function Z depends on an effective Hamiltonian

$$H_{eff} = H_d + \frac{1}{2}\sum_{j=L,R}\sum_{nm}\left(\Gamma^{(j)}_{nm} e^{i\phi_j} d_{n\downarrow} d_{m\uparrow} + \text{h.c.}\right) \tag{3.10}$$

Introducing the basis $\{|1,\uparrow\rangle, |2,\downarrow\rangle, |1,\downarrow\rangle, |2,\uparrow\rangle\}$, the single particle matrix h reads:

$$h = \begin{pmatrix} \mu+\epsilon+B & -\alpha\sin\chi & 0 & i\alpha\cos\chi \\ -\alpha\sin\chi & \mu-(\epsilon+B) & i\alpha\cos\chi & 0 \\ 0 & -i\alpha\cos\chi & \mu+\epsilon-B & \alpha\sin\chi \\ -i\alpha\cos\chi & 0 & \alpha\sin\chi & \mu-(\epsilon-B) \end{pmatrix} \tag{3.11}$$

Assuming $\mu = 0$ without losing in generality, we can write the effective Hamiltonian

$$\begin{aligned} H_{eff} = {} & (\epsilon+B)d^\dagger_{1\uparrow}d_{1\uparrow} - (\epsilon+B)d^\dagger_{2\downarrow}d_{2\downarrow} + (\epsilon-B)d^\dagger_{1\downarrow}d_{1\downarrow} - (\epsilon-B)d^\dagger_{2\uparrow}d_{2\uparrow} \\ & + \alpha\sin\chi(d^\dagger_{1\downarrow}d_{2\uparrow} - d^\dagger_{1\uparrow}d_{2\downarrow} + \text{h.c.}) + \alpha\cos\chi(id^\dagger_{1\uparrow}d_{2\uparrow} - id^\dagger_{1\downarrow}d_{2}\downarrow + \text{h.c.}) \\ & + (\Delta_1(\phi)e^{i\theta_1(\phi)}d^\dagger_{2\uparrow}d^\dagger_{1\downarrow} + \text{h.c.}) + (\Delta_2(\phi)e^{i\theta_2(\phi)}d^\dagger_{1\uparrow}d^\dagger_{2\downarrow} + \text{h.c.}) \\ & + e^{\lambda}(\rho(\phi)e^{i\eta(\phi)}d_{1\downarrow}d_{1\uparrow} + \text{h.c.}) + e^{-\lambda}(\rho(\phi)e^{i\eta(\phi)}d_{2\downarrow}d_{2\uparrow} + \text{h.c.}) \end{aligned} \tag{3.12}$$

From the hybridization matrices (3.8) and from (3.10) we get the complex-valued effective pairing amplitude $\Delta_1 e^{i\theta_1} = \frac{1}{2}\sum_j \gamma_j e^{-i(\phi_j+\delta_j)}$. Introducing $\gamma \equiv (\gamma_L +$

$\gamma_R)/2$, we may gauge away the overall phase $\sum_j(\phi_j+\delta_j)/2$

$$\begin{aligned}
\frac{1}{2}[\gamma_L e^{-i(\phi_L+\delta_L)}+\gamma_R e^{-i(\phi_R+\delta_R)}] &= \\
&= \frac{1}{2}e^{-i(\phi_L+\delta_L+\phi_R+\delta_R)/2}[\gamma_L e^{-i(\phi_L+\delta_L-\phi_R-\delta_R)/2}+\gamma_R e^{-i(\phi_R+\delta_R-\phi_L-\delta_L)/2} \\
&= \frac{1}{2}e^{-i\Theta}\left[\gamma_L\cos\left(\frac{\phi+\delta}{2}\right)-i\gamma_L\sin\left(\frac{\phi+\delta}{2}\right)\right. \\
&\left.+\gamma_R\cos\left(\frac{\phi+\delta}{2}\right)+i\gamma_R\sin\left(\frac{\phi+\delta}{2}\right)\right] \\
&= \frac{1}{2}e^{-i\Theta}\left[(\gamma_R+\gamma_L)\cos\left(\frac{\phi+\delta}{2}\right)+i(\gamma_R-\gamma_L)\sin\left(\frac{\phi+\delta}{2}\right)\right]
\end{aligned}$$

where we have used $\Theta=(\phi_L+\delta_L+\phi_R+\delta_R)/2$ and $\phi=\phi_L-\phi_R$. We can now find

$$\begin{aligned}
\Delta_1(\phi) &= \frac{1}{2}\sqrt{\cos^2\left(\frac{\phi+\delta}{2}\right)(\gamma_R+\gamma_L)^2+\sin^2\left(\frac{\phi+\delta}{2}\right)(\gamma_R-\gamma_L)^2} \\
&= \frac{1}{2}\sqrt{(\gamma_L+\gamma_R)^2-4\gamma_L\gamma_R\sin^2\left(\frac{\phi+\delta}{2}\right)} \\
&= \frac{1}{2}(\gamma_L+\gamma_R)\sqrt{1-4\frac{\gamma_L\gamma_R}{(\gamma_L+\gamma_R)^2}\sin^2\left(\frac{\mathrm{phi}+\delta}{2}\right)} \\
&= \gamma\sqrt{1-T_0\sin^2\left(\frac{\phi+\delta}{2}\right)} \qquad (3.13)
\end{aligned}$$

$$T_0 = 4\frac{\gamma_L\gamma_R}{(\gamma_L+\gamma_R)^2} \qquad (3.14)$$

$$\begin{aligned}
\theta_1(\phi) &= \tan^{-1}\left[\frac{\sin\left(\frac{\phi+\delta}{2}\right)(\gamma_R+\gamma_L)}{\cos\left(\frac{\phi+\delta}{2}\right)(\gamma_L+\gamma_R)}\right] \\
&= \tan^{-1}\left[\frac{\gamma_R-\gamma_L}{\gamma_L+\gamma_R}\tan\left(\frac{\phi+\delta}{2}\right)\right] \qquad (3.15)
\end{aligned}$$

In an analogous manner, we have

$$\Delta_2(\phi) = \gamma\sqrt{1-T_0\sin^2\left(\frac{\phi-\delta}{2}\right)} \qquad (3.16)$$

$$\theta_2(\phi) = \tan^{-1}\left[\frac{\gamma_R-\gamma_L}{\gamma_R+\gamma_L}\tan\left(\frac{\phi-\delta}{2}\right)\right] \qquad (3.17)$$

$$\rho(\phi) = \gamma\sqrt{1-T_0\sin^2\left(\frac{\phi}{2}\right)} \qquad (3.18)$$

$$\eta(\phi) = \tan^{-1}\left[\frac{\gamma_R-\gamma_L}{\gamma_R+\gamma_L}\tan\left(\frac{\phi}{2}\right)\right] \qquad (3.19)$$

It is easy to see that those amplitudes and phases parameters differ one from another in their dependence on the relative inter orbital phase δ. Defining the spinor $\mathbf{D} = (d_{1\uparrow}, d_{2\downarrow}, d_{1\downarrow}, d_{2\uparrow}, d1\uparrow^{\dagger}, d_{2\downarrow}^{\dagger}, d_{1\downarrow}^{\dagger}, d_{2\uparrow}^{\dagger})^{T}$, we now write the Hamiltonian in matricial form, so that $H_{eff} = \mathbf{D}^{\dagger} H \mathbf{D}$, where H reads

$$H = \begin{pmatrix}
\frac{\epsilon+B}{2} & -\frac{\alpha}{2}\sin\chi & 0 & i\frac{\alpha}{2}\cos\chi & 0 & \frac{\Delta_2}{2}e^{i\theta_2} & \frac{\rho}{2}e^{-i\eta+\lambda} & 0 \\
-\frac{\alpha}{2}\sin\chi & -\frac{\epsilon+B}{2} & i\frac{\alpha}{2}\cos\chi & 0 & -\frac{\Delta_2}{2}e^{i\theta_2} & 0 & 0 & -\frac{\rho}{2}e^{-i\eta-\lambda} \\
0 & -i\frac{\alpha}{2}\cos\chi & \frac{\epsilon-B}{2} & \frac{\alpha}{2}\sin\chi & -\frac{\rho}{2}e^{-i\eta+\lambda} & 0 & 0 & -\frac{\Delta_1}{2}e^{i\theta_1} \\
-i\frac{\alpha}{2}\cos\chi & 0 & \frac{\alpha}{2}\sin\chi & -\frac{\epsilon-B}{2} & 0 & \frac{\rho}{2}e^{-i\eta-\lambda} & \frac{\Delta_1}{2}e^{i\theta_1} & 0 \\
0 & -\frac{\Delta_2}{2}e^{-i\theta_2} & -\frac{\rho}{2}e^{i\eta+\lambda} & 0 & -\frac{\epsilon+B}{2} & \frac{\alpha}{2}\sin\chi & 0 & i\frac{\alpha}{2}\cos\chi \\
\frac{\Delta_2}{2}e^{-i\theta_2} & 0 & 0 & \frac{\rho}{2}e^{i\eta-\lambda} & \frac{\alpha}{2}\sin\chi & \frac{\epsilon+B}{2} & i\frac{\alpha}{2}\cos\chi & 0 \\
\frac{\rho}{2}e^{i\eta+\lambda} & 0 & 0 & \frac{\Delta_1}{2}e^{-i\theta_1} & 0 & -i\frac{\alpha}{2}\cos\chi & -\frac{\epsilon-B}{2} & -\frac{\alpha}{2}\sin\chi \\
0 & -\frac{\rho}{2}e^{i\eta-\lambda} & -\frac{\Delta_1}{2}e^{-i\theta_1} & 0 & -i\frac{\alpha}{2}\cos\chi & 0 & -\frac{\alpha}{2}\sin\chi & \frac{\epsilon-B}{2}
\end{pmatrix} \tag{3.20}$$

3.2 Current-phase relation

In order to study the Josephson current in relation to the parameters characterizing the dot Hamiltonian, it is helpful to write the BdG transformed Hamiltonian

$$H'_{eff} = \sum_i E_i(\phi)\zeta_i^{\dagger}\zeta_i \tag{3.21}$$

We then have

$$I(\phi) = \sum_i \frac{\partial E_i(\phi)}{\partial \phi}[\Theta(-E_i)] \tag{3.22}$$

Where Θ is the Heaviside step function.

Due to the fact that the matrix H (3.20) leads to a characteristic polynomial of 8^{th} grade, and, hence, its eigenvectors are analytically complicated to compute, we numerically found both the eigenvalues and the current. In the following sections, we are analyzing how the current-phase relation (CPR) changes as we vary the parameters χ, λ, α, ϵ, B, T_0 (i.e. γ_L, γ_R) and δ.

3.2.1 Varying χ

To the fixed terms of this section, we assign the values $\delta = \lambda = 0$, $\gamma_L = 0.45$, $\gamma_R = 0.55$ ($T_0 = 0.99$), $\alpha = 0.4\gamma$. Moreover, we take $\epsilon = B$ and look at the limits for small and large ϵ. We report the spectra and the relative current.

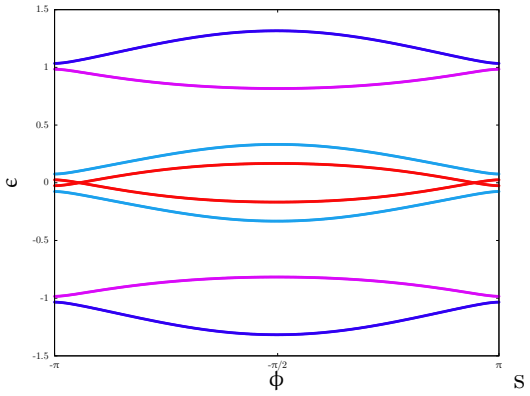

(a) spectrum for $\chi = \pi/6$

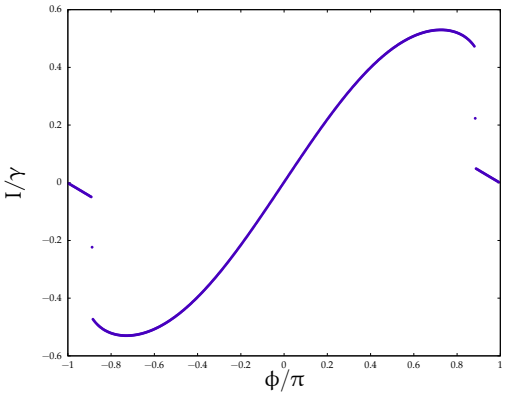

(b) current for $\chi = \pi/6$

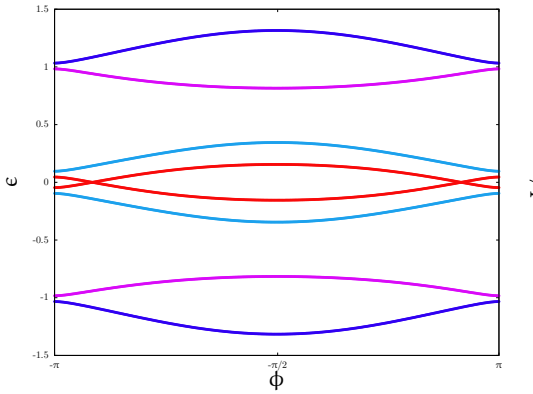

(c) spectrum for $\chi = \pi/4$

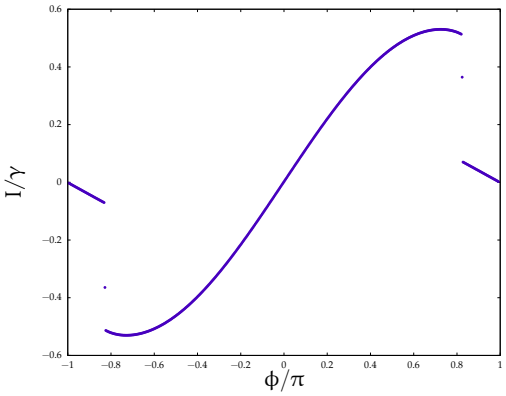

(d) current for $\chi = \pi/4$

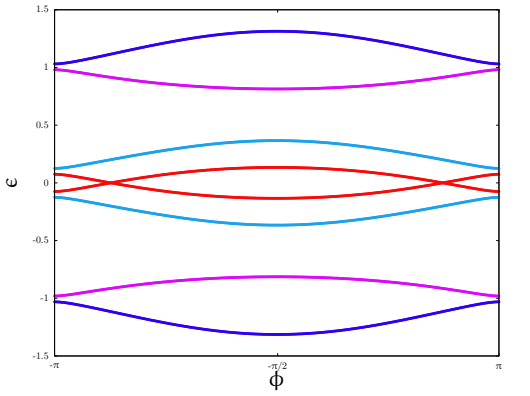

(e) spectrum for $\chi = \pi/2$

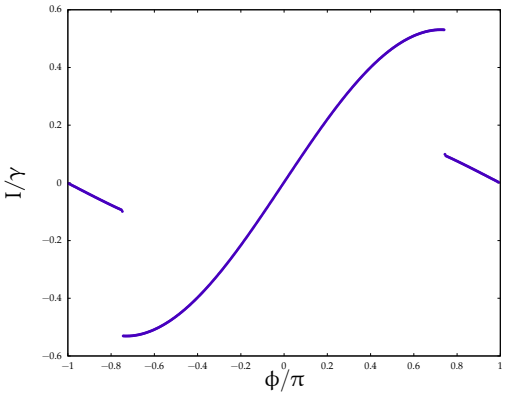

(f) current for $\chi = \pi/2$

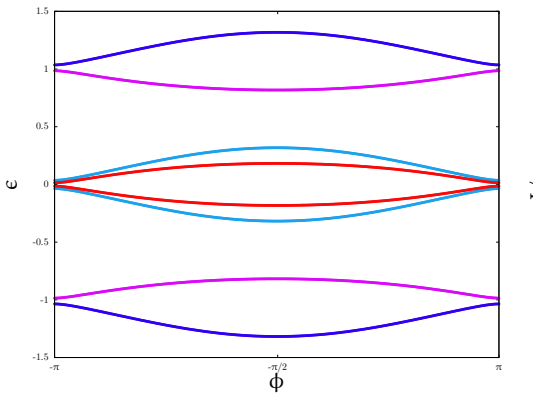

(g) spectrum for $\chi = \pi$

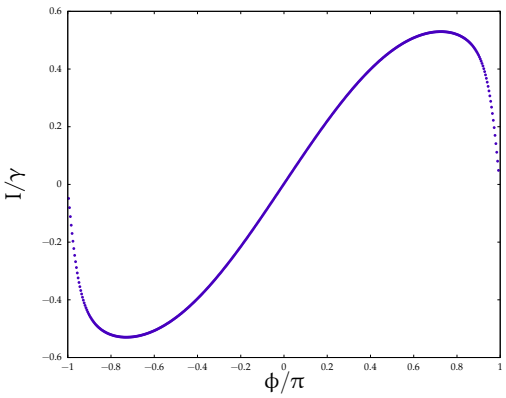

(h) current for $\chi = \pi$

Figure 3.1: Graphics for different χ values in the small ϵ limit

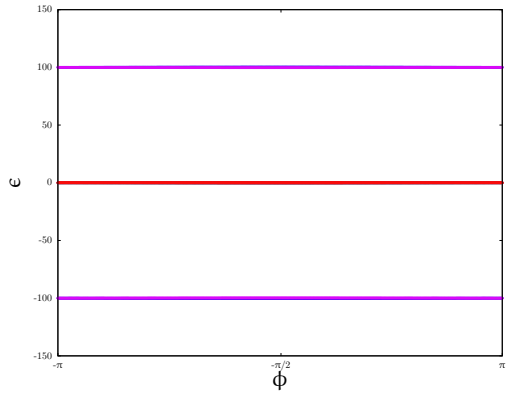

(a) spectrum for $\chi = \pi/6$

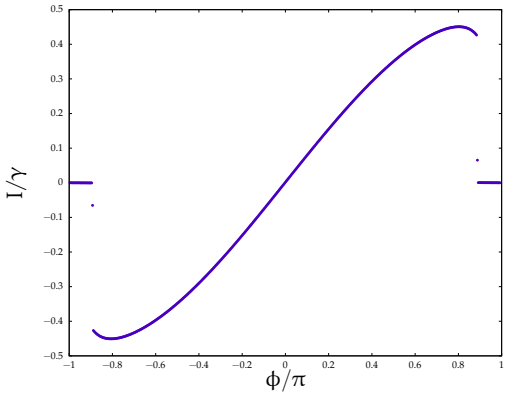

(b) current for $\chi = \pi/6$

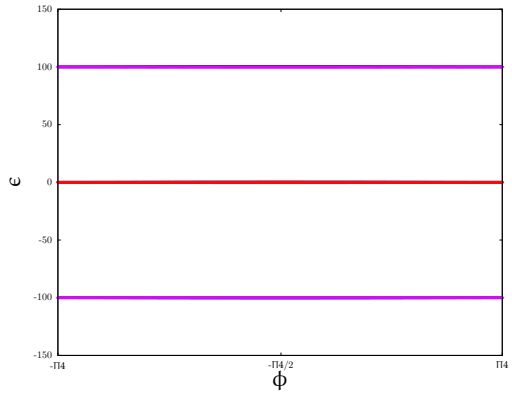

(c) spectrum for $\chi = \pi/4$

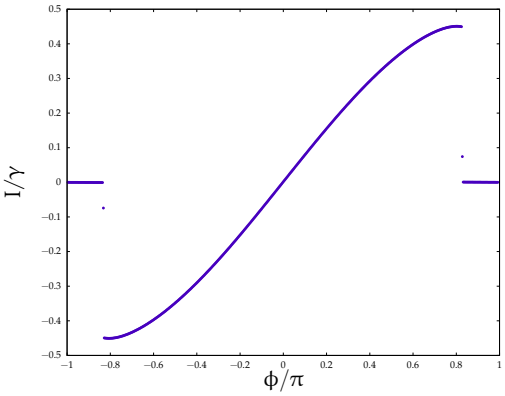

(d) current for $\chi = \pi/4$

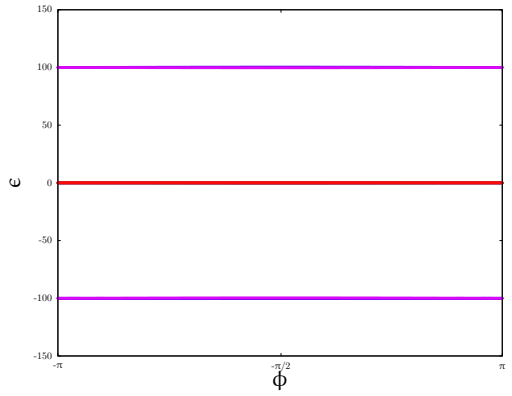

(e) spectrum for $\chi = \pi/2$

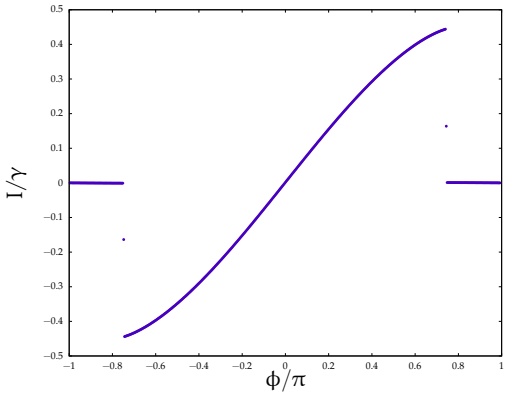

(f) current for $\chi = \pi/2$

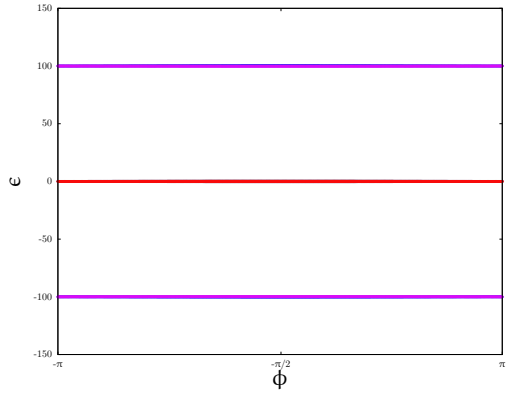

(g) spectrum for $\chi = \pi$

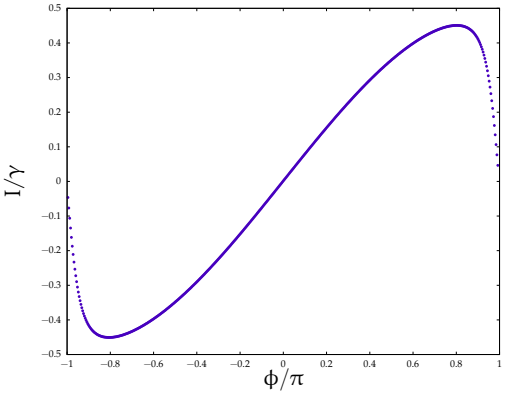

(h) current for $\chi = \pi$

Figure 3.2: Graphics for different χ values in the large ϵ limit

We immediately see the presence of a discontinuity in the current for $\chi = \pi/6, \pi/4, \pi/2$, while the function is continuous when $\chi = \pi$. Physically, this means that the flat part is bigger when the SOC field is orthogonal to the Zeeman field, while it vanishes when they are parallel, i.e. the SOC field is just "added" to the magnetic one.Looking at the spectra, we recognize that the presence of the jump is due to the overlapping in zero of the two lowest energy bands (red lines in the graphs). Moreover, the straight parts at the endings of the graphics increases with χ until it reaches the value $\chi = \pi/2$, then they decrease again, vanishing when $\chi = \pi$. The main difference between the small and the large limit is that the straight parts are horizontal in the latter case, which point us to the typical step function shape. Furthermore, we remark that the spectra are exactly the same, near zero, in both cases, even if it is not visible from the plots reported here.

3.2.2 Varying λ

We take the fixed values to be as in the previous section, setting the value $\chi = \pi/2$ and varying the λ value. Physically, λ is related to the hopping modulus $|t_{i,j}|^2$, $i = 1, 2$ and $j = L, R$, thus it gives an amplitude of the tunneling probability between the j lead and the ith dot level. Again, we look at the small and the large limit for the energy. Furthermore, we are only considering the symmetric case $\lambda_L = \lambda_R$, so that the Hamiltonian can be written as in (3.20). We analysed the values $\lambda = 0.01, 0.1, 0.5, 1$.

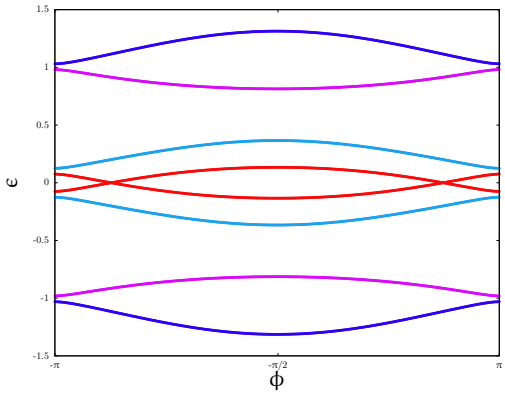

(a) spectrum for $\lambda = 0.01$

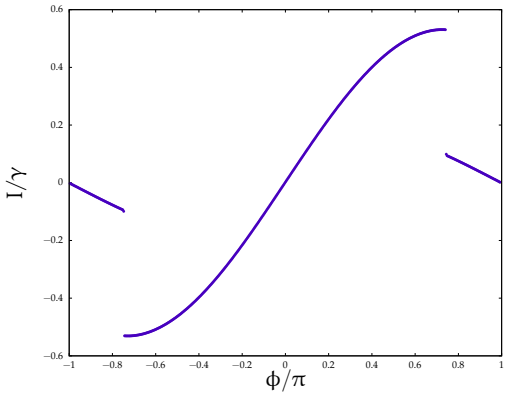

(b) current for $\lambda = 0.01$

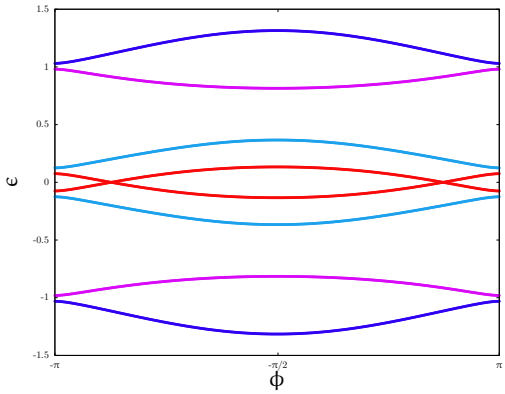

(c) spectrum for $\lambda = 0.1$

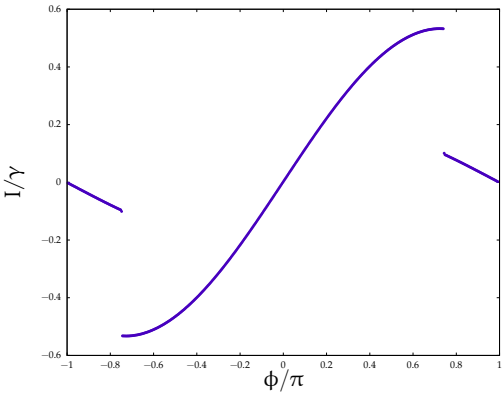

(d) current for $\lambda = 0.1$

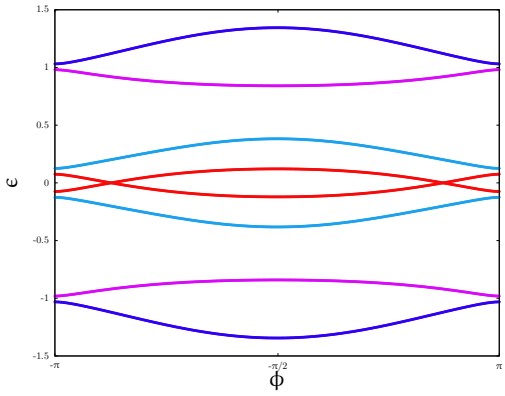

(e) spectrum for $\lambda = 0.5$

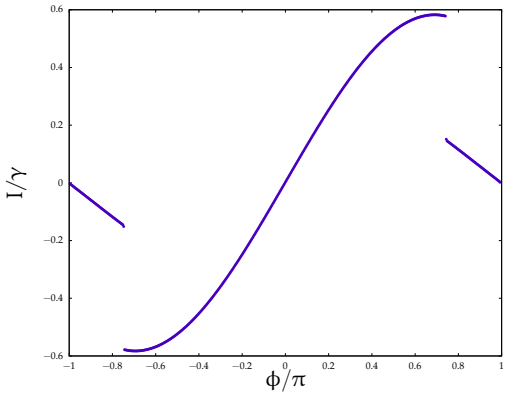

(f) current for $\lambda = 0.5$

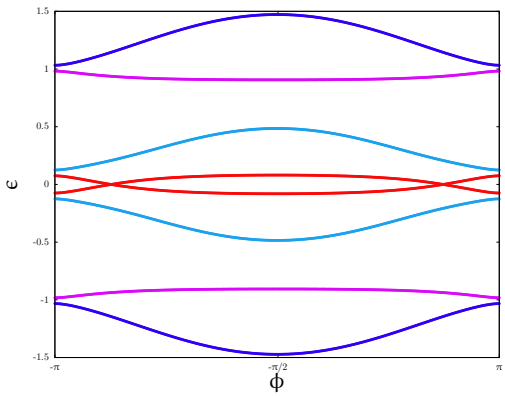

(g) spectrum for $\lambda = 1$

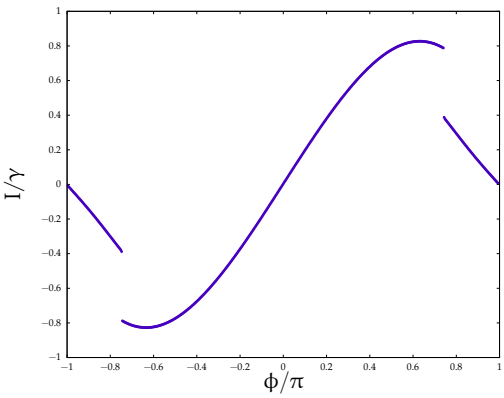

(h) current for $\lambda = 1$

Figure 3.3: Graphics for different λ values in the small ϵ limit

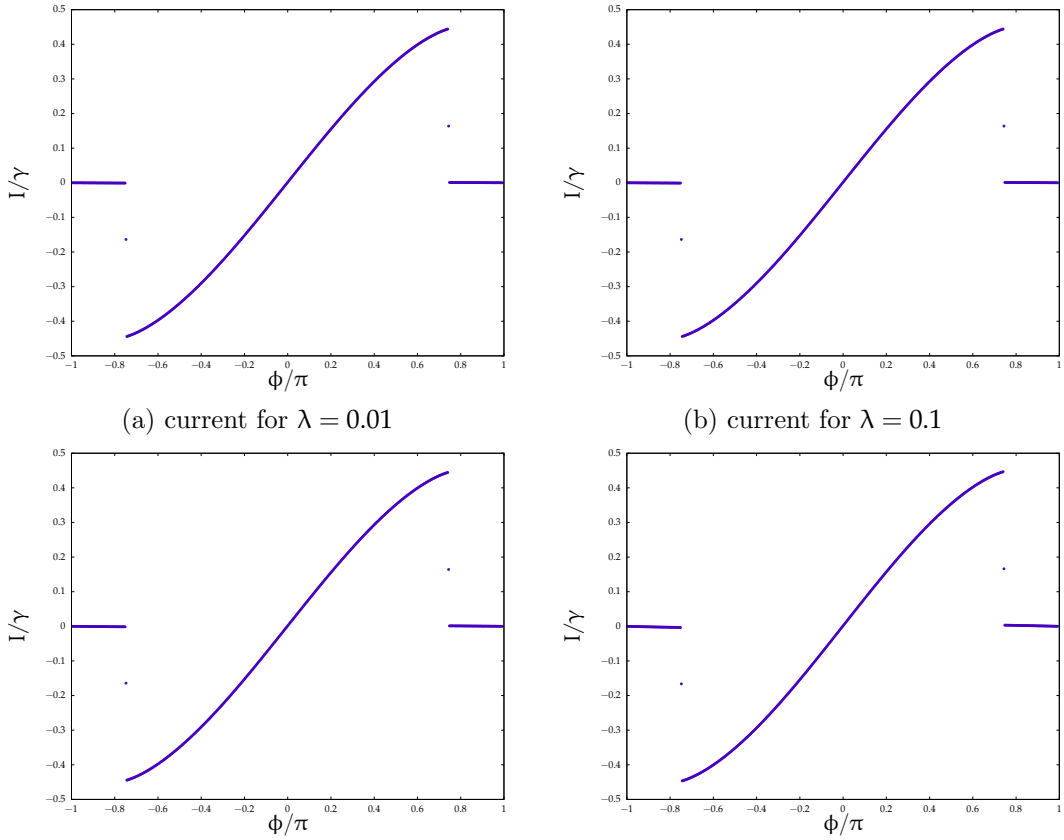

(a) current for $\lambda = 0.01$

(b) current for $\lambda = 0.1$

(c) current for $\lambda = 0.5$

(d) current for $\lambda = 1$

Figure 3.4: Graphics for different λ values in the large ϵ limit

In the large limit, we did not reported the spectra as they are not helpful for our analyis, given their flattening shape, as in the large limit case seen in the previous section.

The first thing to mention, for the case here in consideration, is that the jumping form of the current is conserved. Moreover, in the small limit we see that the angle with the horizontal increases with lambda. Concerning the large limit, we note that the current shape is not affected by the changes in the λ value.

3.2.3 Varying α

We now want to investigate how the spin-orbit coupling strength affects the current-phase relation. We fix the other values as in the previous sections and consider $\alpha = 0.1\,\gamma, \gamma, 10\,\gamma$. As already done, we look at the two limits for the energy scale.

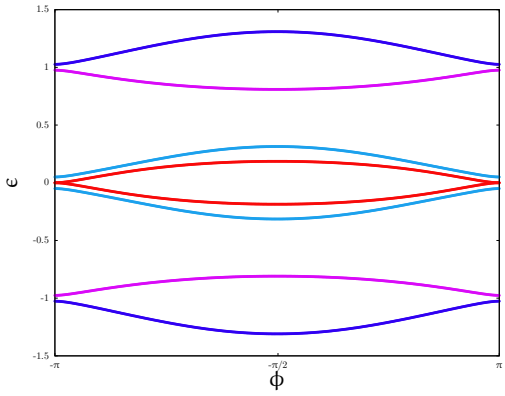

(a) spectrum for $\alpha = 0.1\gamma$

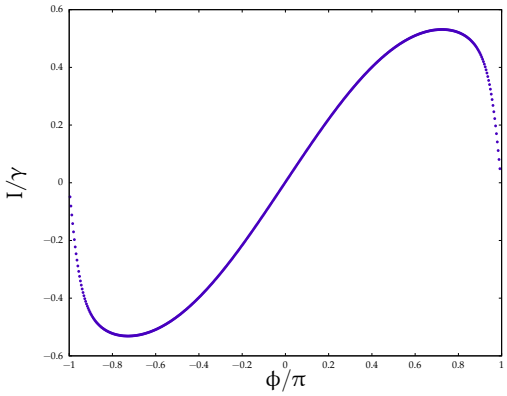

(b) current for $\alpha = 0.1\gamma$

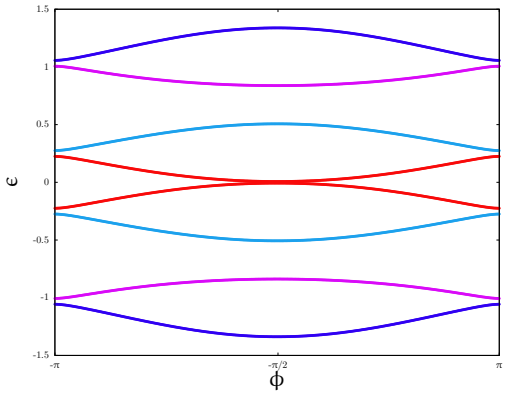

(c) spectrum for $\alpha = \gamma$

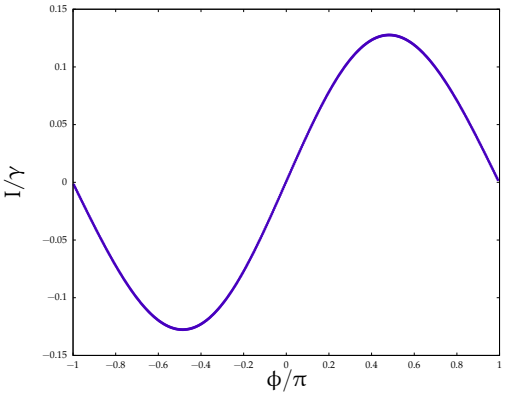

(d) current for $\alpha = \gamma$

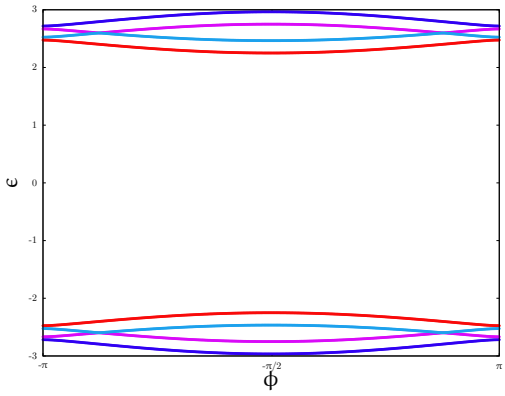

(e) spectrum for $\alpha = 10\gamma$

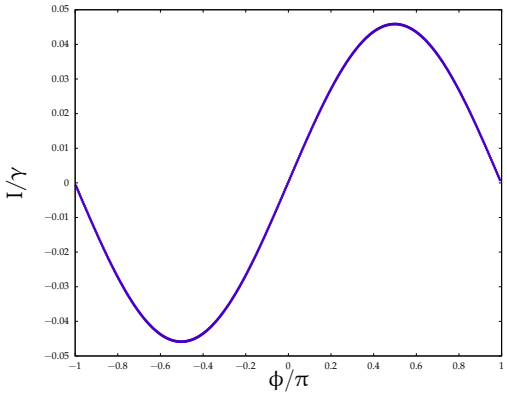

(f) current for $\alpha = 10\gamma$

Figure 3.5: Graphics for different α values in the small ϵ limit

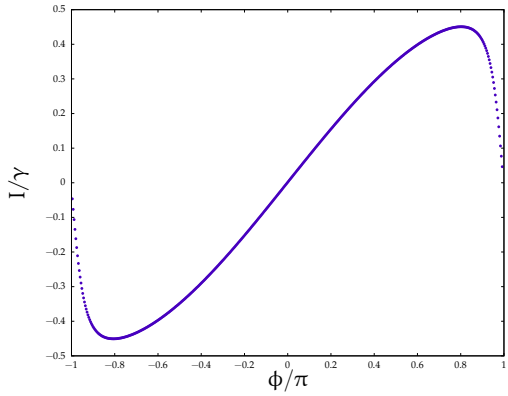

(a) current for $\alpha = 0.1\gamma$

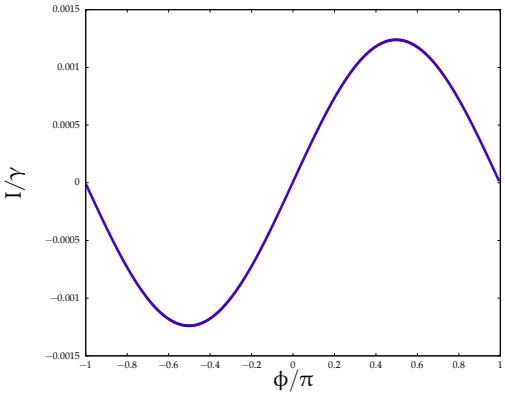

(b) current for $\alpha = \gamma$

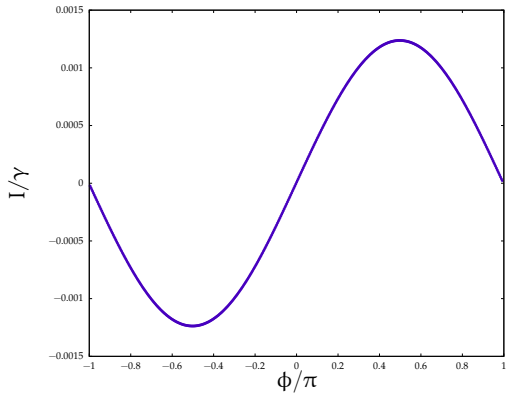

(c) current for $\alpha = 10\gamma$

Figure 3.6: Graphics for different α values in the large ϵ limit

As α varies, the current shape varies, but, for the values here analyzed and with the other parameter fixed such that $T_0 = 0.99$, it remains continuous (see 3.2.1 for an intermediate case between $\alpha = 0.1\,\gamma$ and $\alpha = \gamma$ that shows a jump discontinuity). A better reading may be done looking at the spectra. We see that there are no overlappings in zero for the lowest levels. Besides, we note there is a shifting of the lowest levels towards highest values. Looking at the first and the second case, we notice a change in the convexity of the lowest energy level (red line): while "migrating" as a function of α, the two levels overlaps and that alters the current shape, causing the discontinuity. Furthermore, we may say that the SOC affects two (four) energy levels (red and light-blue lines), while changing the ϵ, B values has effect on the other two (four) energy levels (violet and blue lines).

3.2.4 Varying ϵ and B

In the previous sections we have considered the case $\epsilon = B$ and looked at how the current changed in the small ($\epsilon = 1$) and large ($\epsilon = 100$) limit. Now we want to see how the current behave when ϵ and B take different values. The other parameters are fixed as before.

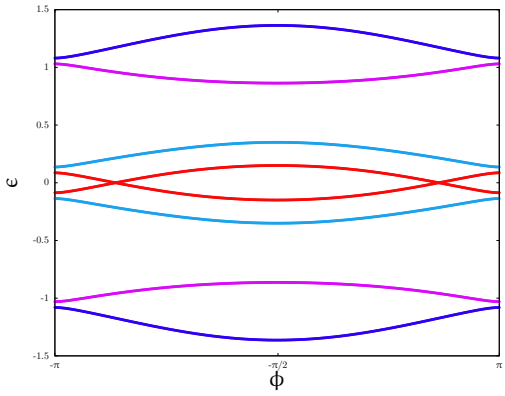

(a) spectrum for $B = 1.1$, $\epsilon = 1$

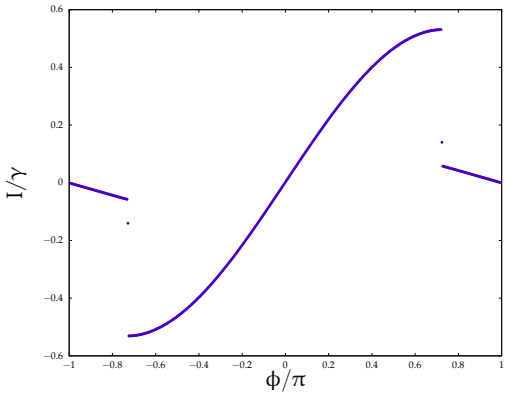

(b) current for $B = 1.1$, $\epsilon = 1$

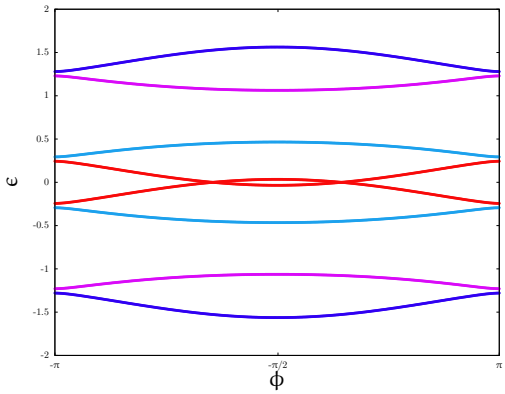

(c) spectrum for $B = 1.5$, $\epsilon = 1$

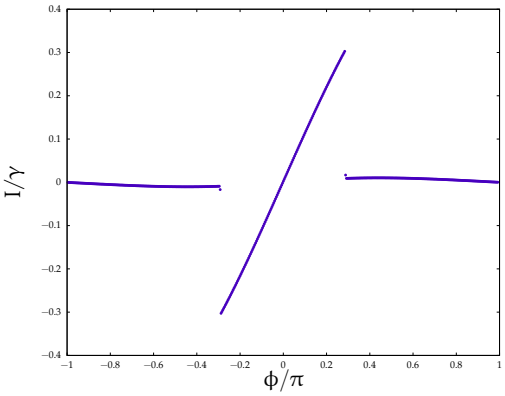

(d) current for $B = 1.5$, $\epsilon = 1$

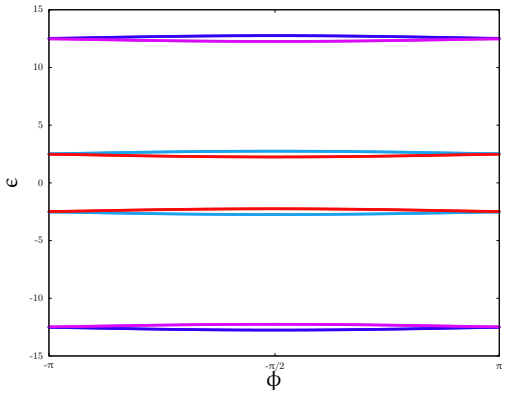

(e) spectrum for $B = 15$, $\epsilon = 10$

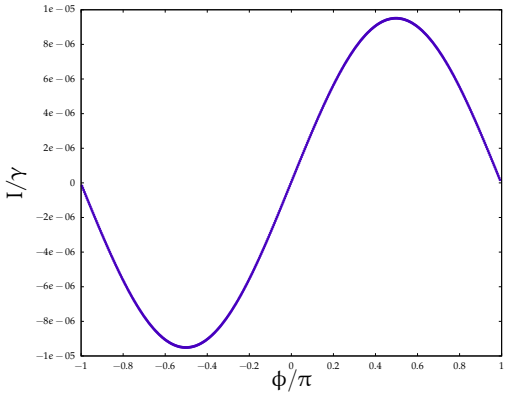

(f) current for $B = 15$, $\epsilon = 10$

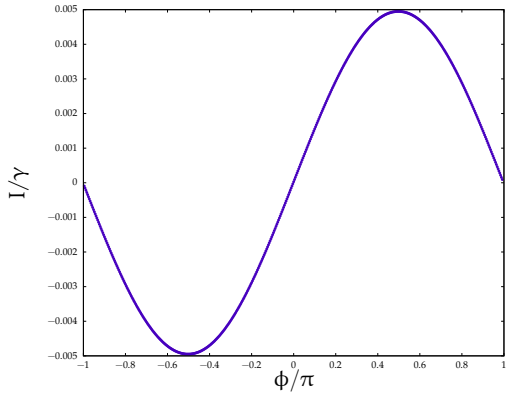

(a) current for $B = 10$, $\epsilon = 50$

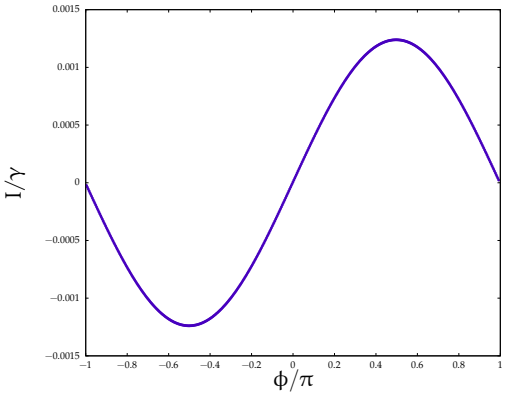

(b) current for $B = 50$, $\epsilon = 10$

We immediately notice that the discontinuity in the current and the overlappings in the spectra are still present while the magnitudes of ϵ and B are somehow comparable to that of the SOC strength α and their difference $|\epsilon - B|$ is of lower order in respect of their magnitude, but as fast as they become enough large to well separate the energy bands, and their difference is comparable to their magnitude, the discontinuity is no more present.

3.2.5 Varying T_0

We here vary the relation between g_L and g_R. We fix $\alpha = 0.8\,\gamma$, with γ depending on the γ_j. We coupled the different values as $\gamma_L = \gamma_R = 0.55$, $T_0 = 1$, $\gamma_L = 0.2$, $\gamma_R = 0.5$, $T_0 \approx 0.8$, $\gamma_L = 0.2$, $\gamma_R = 0.7$, $T_0 \approx 0.7$ and $\gamma_L = 0.2$, $\gamma_R = 0.9$, $T_0 \approx 0.6$.

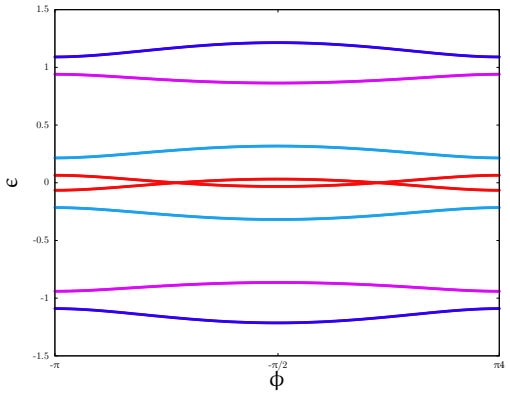

(a) spectrum for $T_0 \approx 0.6$

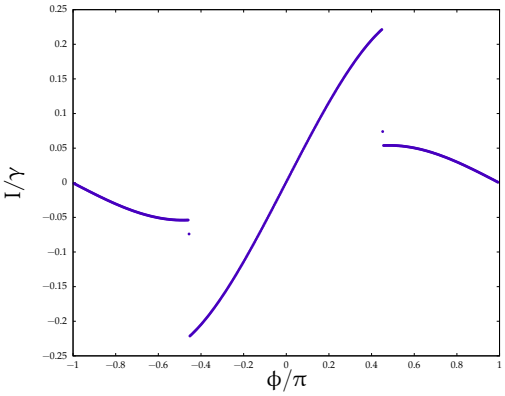

(b) current for $T_0 \approx 0.6$

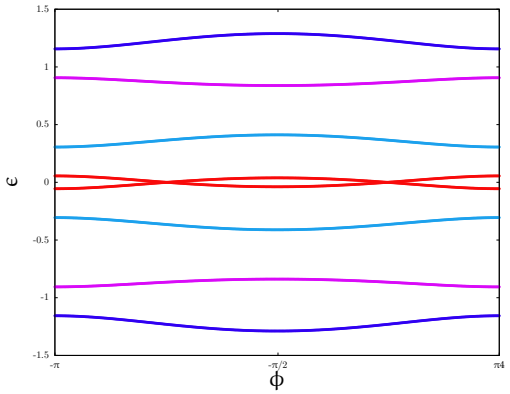

(c) spectrum for $T_0 \approx 0.7$

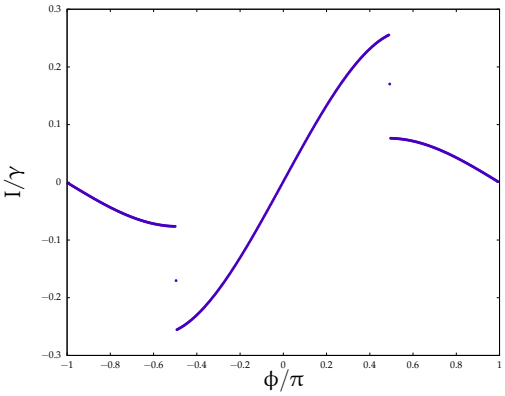

(d) current for $T_0 \approx 0.7$

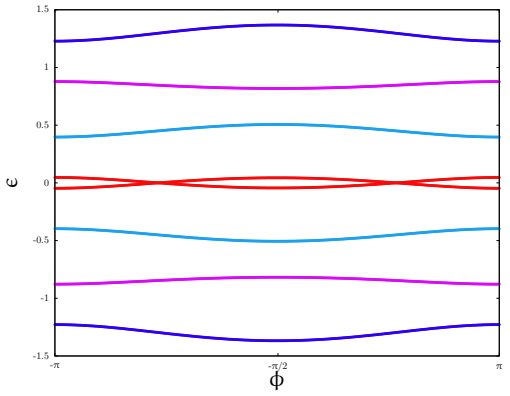

(e) spectrum for $T_0 \approx 0.8$

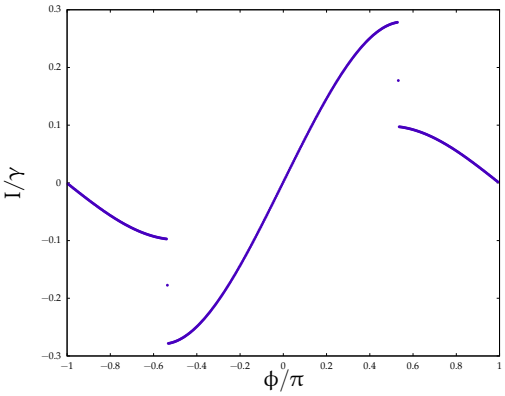

(f) current for $T_0 \approx 0.8$

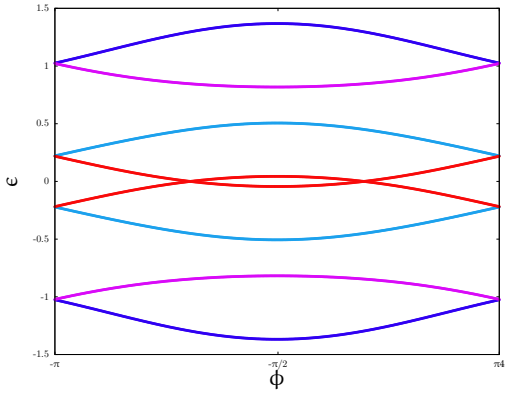

(g) spectrum for $T_0 = 1$

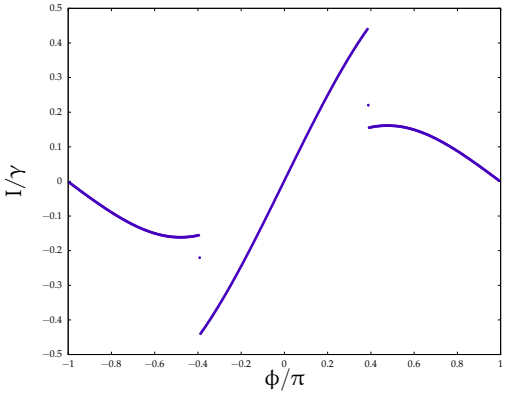

(h) current for $T_0 = 1$

Figure 3.9: Graphics for different values of T_0 in the small ϵ limit

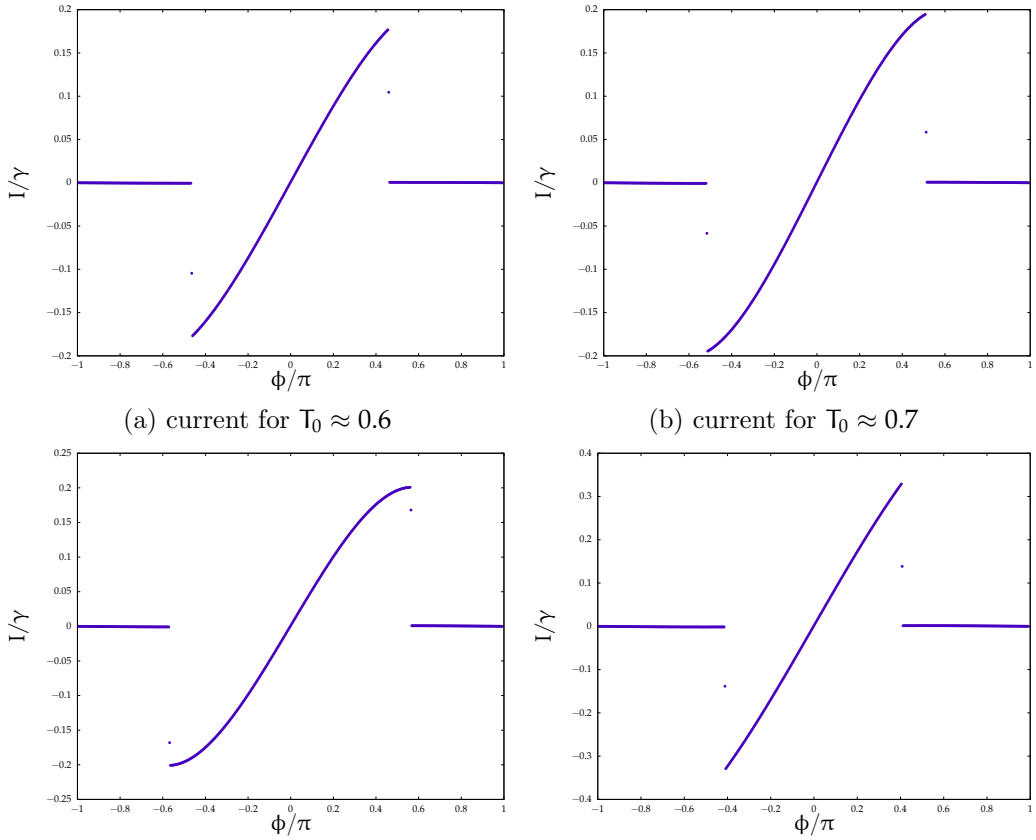

(a) current for $T_0 \approx 0.6$

(b) current for $T_0 \approx 0.7$

(c) spectrum for $T_0 \approx 0.8$

(d) current for the $T_0 = 1$

Figure 3.10: Graphics for different values of T_0 in the large ϵ limit

We notice that the overlappings in the spectra are present, but the form of the two lowest energies (red lines) is extremely different in the symmetrical case. Furthermore, we again have the discontinuity in the current and the fattening in the large energy limit. We also discern a diverse current shape in the large limit for the symmetrical case. In fact, the not-constant part is almost a straight line. We here want to remark that, even if we are not reporting the graphics, if we put $\alpha = 0.4\,\gamma$ as in the previous sections, we have a continuous current. Thus, the relation between α and T_0 is determinant for the discontinuity to be present.

3.2.6 Varying δ

While varying δ, we had to be careful in handling the divergence due to the present of the tangent in (**??**). We fix all the values as usual and look at the cases $\delta = \pi/6$, $\delta = \pi/4$, $\delta = \pi/3$, $\delta = 2\pi/3$, $\delta = 3\pi/4$, $\delta = 5\pi/6$. We also wanted to analyze the case $\delta = \pi/2$. In order to do so, we took $\delta = \pi/2 + \pi/100$ and avoided the divergence due to $\tan(\pi/2) = \infty$. We report the plot for a spectrum in the small energy limit as indicative of the distinct shape of the energy levels in this case and its relative current plot and the graphs relative to the different values of δ for the current in the large energy limit.

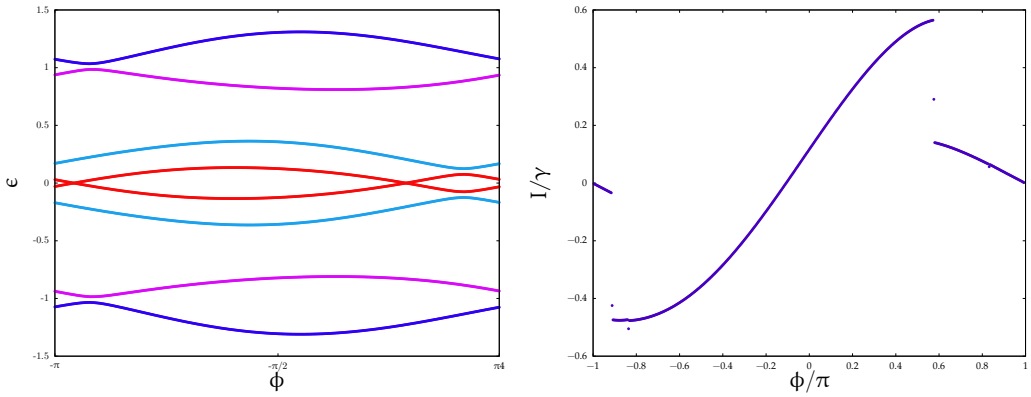

(a) spectrum for $\delta = \pi/6$

(b) current for $\delta = \pi/6$

Figure 3.11: Illustrative plots for the small energy limit

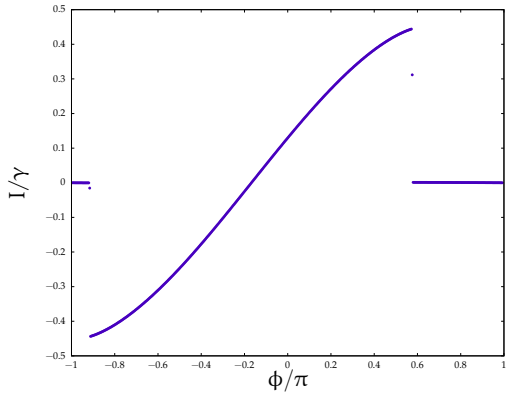

(a) current for $\delta = \pi/6$

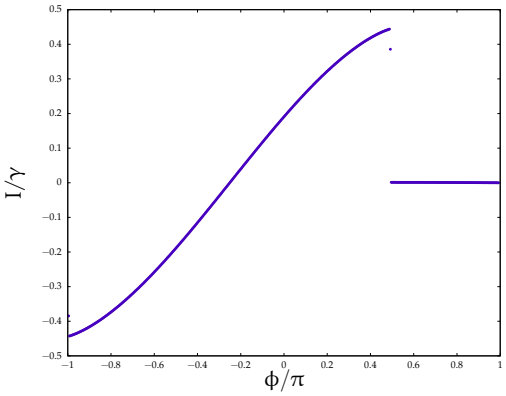

(b) current for $\delta = \pi/4$

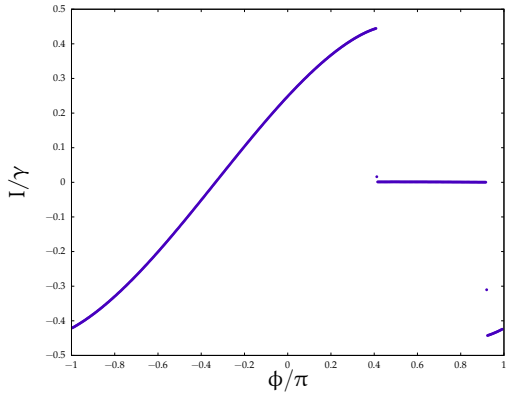

(c) spectrum for $\delta = \pi/3$

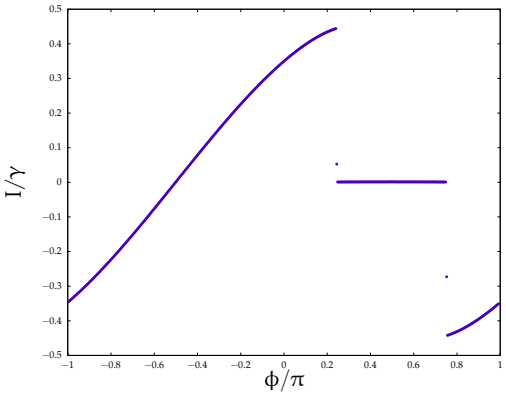

(d) current for the $\delta = \pi/2 + \pi/1000$

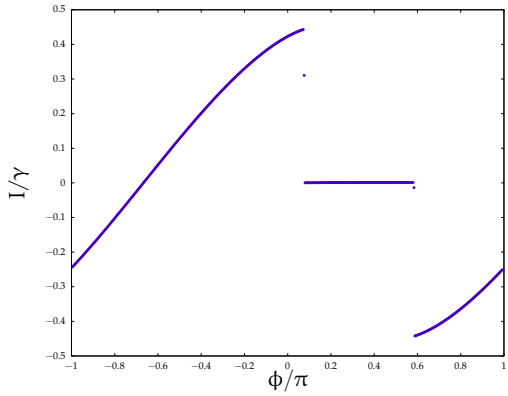

(e) spectrum for $\delta = 2\pi/3$

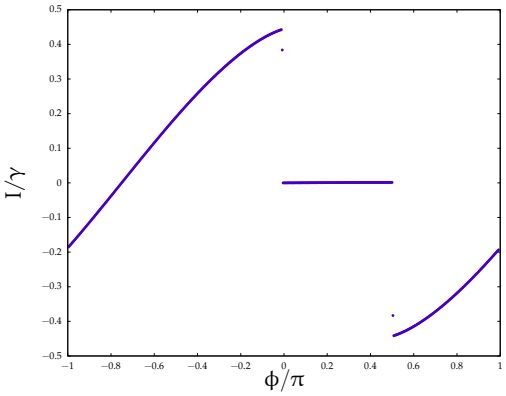

(f) current for the $\delta = 3\pi/4$

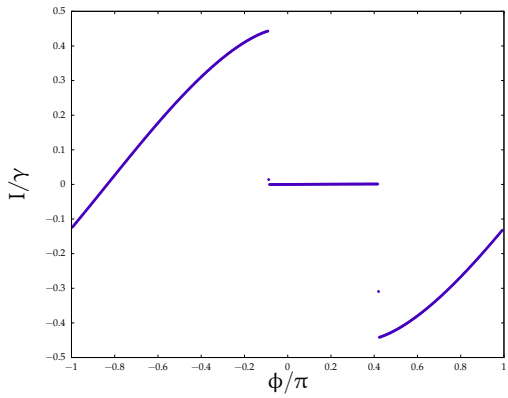

(g) spectrum for $\delta = 5\pi/6$

Figure 3.12: Graphics for different values of δ in the large ϵ limit

Concerning the example for the small energy limit, we see how the overlappings in the spectrum are present and the discontinuity in the current too. The distinct behavior in respect of what has been seen in the previous sections is the horizontal shifting in the spectrum. Moreover, this shifting is easily observed in the reported graphics for the current in the large energy limit: as δ increases, the current shape remains the same while there is a "movement" to the left.

3.3 Physical significance of the current discontinuity

We have seen a discontinuity arises in the current under a certain parameters regime. We now want to relate this phenomenon to its physical cause and significance. In order to do so, we will introduce the concepts and formalism regarding Majorana fermions (MFs) in condensed matter physics, then demonstrate how our system can be mapped into a Kitaev chain in a well defined energy limit.

3.3.1 Majorana quasiparticles in condensed matter physics

Majorana fermions (MFs) are fermionic particles which are their own antiparticles. Whether they exist or not as elementary particles is still unclear. It is conventional, in condensed matter to refer to particular quasiparticles, that shows Majorana characteristic, as Majorana fermions, even if they exhibit a non-Abelian anyonic statistic [4]. Thus, in line with the literature, we will refer, in this text, to those quasiparticles as Majorana fermions. In the case just described, a MF is a quasiparticle which is its 'own hole'. Furthermore, A Majorana particle can be seen as half of a fermion, or in other words, a fermion can be obtained as a superposition of two MFs. We can always split a fermionic wave-function in two parts: a real one and an imaginary one. This may seem as just a mathematical operation without physical significance or consequences: that is true if the MFs are spatially localized and hence their wave-functions overlap significantly, so that they recombine, but if they are spatially separated (or prevented from overlapping) the physical meaning becomes clear. Moreover, such a highly delocalized fermionic state is protected from almost all kinds of decoherence as it is not affected by local perturbations acting on jus one of its Majorana constituent. The state can be manipulated using the fact that MFs have non-Abelian statistics, thus a physical exchange of MFs has a non trivial effect on the state [19].

The simplest Hamiltonian to start with, in looking for a good description for this peculiar particles, is that describing a 1D tight-binding chain with p-wave superconducting pairing, as first introduced by Kitaev (Kitaev chain):

$$\mathcal{H}_{\text{chain}} = -\mu \sum_{i=1}^{N} n_i - \sum_{i=1}^{N-1} (t c_i^\dagger c_{i+1} + \Delta c_i c_{i+1} + \text{h.c.}) \tag{3.23}$$

where μ is the chemical potential, c_i is the electron annihilation operator for site i and $n_i = c_i^\dagger c_i$ is the associated number operator. For simplicity, we assume the hopping t and the superconducting gap Δ to be the same for all sites. Then, we can choose the superconducting phase ϕ to be zero so that $\Delta = |\Delta|$. It is important to

note that time reversal symmetry is broken in the Hamiltonian (3.23), since we have suppressed the spin label thus considering just one value for the spin projection: this symmetry breaking is fundamental for MFs as we now that, in the time sector, we can consider the antiparticles to be the particles going back in time, so, if the system is time-invariant, we cannot tell the particles from the antiparticles. Going back to our systems, the superconducting pairing is non-standard, since it couples electrons with the same spin. Moreover, electrons on neighboring sites are paired.

In order to write eq. (3.23) in terms of Majorana operators we define two Hermitian operators as

$$\gamma_{i,1} = c_i^\dagger + c_i \tag{3.24a}$$

$$\gamma_{i,2} = i(c_i^\dagger - c_i) \tag{3.24b}$$

And, inverting, we see that this gives $\gamma_{i,1}$ and $\gamma_{i,2}$ as "real" and "imaginary" parts of the electrons operators

$$c_i = \frac{1}{2}(\gamma_{i,1} + i\gamma_{i,2}) \tag{3.25a}$$

$$c_i^\dagger = \frac{1}{2}(\gamma_{i,1} - i\gamma_{i,2}) \tag{3.25b}$$

From their definition, these operators are Hermitian and, therefore, Majorana operators.

To better understand Majorana physics, we consider the case $\mu = 0$, $t = \Delta$. Inserting eq (3.25a) and (3.25b) into the Hamiltonian (3.23), we have

$$\begin{aligned}
\mathcal{H}_{\text{chain}} &= -t \sum_{i=1}^{N-1} (c_i^\dagger c_{i+1} + c_i c_{i+1} + c_{i+1}^\dagger c_i + c_{i+1}^\dagger c_i^\dagger) \\
&= -\frac{t}{4} \sum_{i=1}^{N-1} [(\gamma_{i,1} - i\gamma_{i,2})(\gamma_{i+1,1} + i\gamma_{i+1,2}) + (\gamma_{i,1} + i\gamma_{i,2})(\gamma_{i+1,1} + i\gamma_{i+1,2}) \\
&+ (\gamma_{i+1,1} - i\gamma_{i+1,2})(\gamma_{i,1} + i\gamma_{i,2}) + (\gamma_{i+1,1} - i\gamma_{i+1,2})(\gamma_{i,1} - i\gamma_{i,2})] \\
&= -it \sum_{i=1}^{N-1} \gamma_{i,2}\gamma_{i+1,1}
\end{aligned} \tag{3.26}$$

And (3.26) is just the diagonalized Hamiltonian. To see it, we can go back to a fermionic representation constructing new "normal" fermions operators $\tilde{c}_i$ by combining Majorana operators on neighboring sites:

$$\tilde{c}_i = (\gamma_{i+1,1} + i\gamma_{i,2})/2 \tag{3.27}$$

We then find

$$-i\gamma_{i,2}\gamma_{i+1,1} = 2\tilde{c}_i^\dagger \tilde{c}_i = 2\tilde{n}_i$$

Therefore

$$\mathcal{H}_{\text{chain}} = 2t \sum_{i=1}^{N-1} \tilde{c}_i^\dagger \tilde{c}_i \tag{3.28}$$

We then see that $\tilde{c}_i$ are annihilation operators corresponding to the eigenstates and the energy cost of creating a $\tilde{c}_i$ fermion is $2t$. We may hence say that the Majorana operators are merely a formal way of rewriting the Hamiltonian and the physical excitations are fermionic states at finite energy, obtained by a superposition of nearest neighbor MFs. So, there appears to be nothing special about eq (3.26). Nevertheless, we notice that the Majorana operators $\gamma_{N,2}$ and $\gamma_{1,1}$, localized at the two ends of the wire, are completely missing from eq. (3.26). We may rearrange this two Majorana operators to describe a single fermionic state

$$\tilde{c}_M = (\gamma_{N,2} + i\gamma_{1,1})/2 \tag{3.29}$$

As the MFs associated to the operators $\gamma_{2,N}$ and $\gamma_{1,1}$ are localized at the two opposite ends of the chain, we conclude that this state is highly non-local and, since the fermion operator is absent from the Hamiltonian, occupying the corresponding state requires zero energy. We know that, normally, superconductors have a non-degenerate ground state consisting of superposition of even-particle-number states (condensate of Cooper pairs). In contrast to this, the Hamiltonian (3.23) allows for an odd number of quasiparticles at zero energy cost. The ground state is thus twofold degenerate: corresponding to have in total an even or odd number of electrons in the superconductor. This property is also called parity and corresponds to the eigenvalue of the number operator associated to the zero-energy fermion, $n_M = \tilde{c}_M^\dagger \tilde{c}_M = 0(1)$ for even (odd) parity.

We have considered only the very special case with $\mu = 0$ and $\Delta = t$. It can be shown that the Majorana end states remain as long as the chemical potential lies within the gap, $|\mu| < 2t$. In this general case the MFs are not completely localized at the ends but decay exponentially away from the edges [19]. Moreover, the MFs remain at zero energy only if the wire is long enough that they do not overlap.

Another, easier, way to see the MFs are zero-energy modes is to notice that we are actually interested in systems where the particles are electrons while the antiparticles are holes. We know that electrons have energy $E > 0$, where we have put $E_F = 0$, and holes have energy $-E$. Then, if we consider the set of fermionic operators $\{\xi(E), \xi^\dagger(E)\}$, the following relation is true

$$\xi(E) = \xi^\dagger(-E)$$

Then, at the Fermi level, we have $\xi = \xi^\dagger$, and we have concluded.

Majorana fermions in condensed matter physics have other peculiar properties, but we are not entering their detail as our work is not related to them and a good dissertation would require way more expertise and space than ours.

3.3.2 Mapping the system to a Kitaev chain

Following the work by Brunetti et al. [21], we now demonstrate how the discontinuity in the current is related to the occurrence of MFs states.

First, we have seen how a peculiar Θ Heaviside function shape occurs in the current form in the large limit, and how the energy scale relation between the SOC, ϵ and B is essential to the overlapping in the spectra and the current jumping

discontinuity. Furthermore, we have considered the connection between B and ϵ in the large limit and observed that the discontinuity vanishes when $B \neq \epsilon$. Thus, we will consider the parameter regime

$$\Delta \gg \epsilon + B \gg \max(\alpha, |\epsilon - B|, \gamma_{L,R}, \mu) \tag{3.30}$$

and $\epsilon = B$, while $\mu = 0$ as already set above. Moreover, we set $\chi = \pi/2$ in order to have a block-diagonal dot Hamiltonian matrix h (3.11). We can now simplify our system noting that the upper-block state $(2,\downarrow)$ is always full, while the state $(1,\uparrow)$ is always empty. We can then write a truncated effective Hamiltonian H'_{eff}, acting only within the lower right block described by the (effectively spinless) fermion operators $d_{1,\downarrow} \equiv d_1$, $d_{2,\uparrow} \equiv d_2$

$$\begin{aligned} H'_{eff} &= (\mu + \epsilon - B) d_1^\dagger d_1 + [\mu - (\epsilon - B)] d_2^\dagger d_2 \\ &+ \left(\alpha d_1^\dagger d_2 + \tilde{\Delta}(\phi) e^{i\theta(\phi)} d_2^\dagger d_1^\dagger + \text{h.c.} \right) \end{aligned} \tag{3.31}$$

The fact that we have dropped the spin indices should point to the Kitaev chain (3.23) and the considerations done in section 3.3.1. Using equations (3.13) (3.14) (3.15), we put $\Delta_1(\phi) \equiv \tilde{\Delta}(\phi)$ and $\theta_1(\phi) \equiv \theta(\phi)$. H'_{eff} can be diagonalized in terms of fermionic Bogoliubov-de Gennes quasiparticle operators

$$\eta_\pm = \frac{1}{2} \left[d_1 + d_2 \pm e^{i\theta} \left(d_1^\dagger - d_2^\dagger \right) \right] \tag{3.32}$$

wich yields

$$H'_{eff} = \sum_\pm E_\pm(\phi) \left(\eta_\pm^\dagger \eta_\pm - \frac{1}{2} \right) \qquad E_\pm = \alpha \pm \tilde{\Delta}(\phi) \tag{3.33}$$

The current phase relation follows from (3.33)

$$I(\phi) = 2\partial_\phi \tilde{\Delta} [\Theta(-E_+) - \Theta(-E_-)] \tag{3.34}$$

Where Θ is the Heaviside function. Notice that $I = 0$ for $\tilde{\Delta} < \alpha$. as both energies $E_\pm = \alpha \pm \tilde{\Delta}$ have the same sign. Therefore

$$\begin{aligned} I(\phi) &= \Theta(\tilde{\Delta}(\phi) - \alpha) I_0(\phi) \\ I_0(\phi) &= \frac{\gamma}{2} \frac{T_0 \sin(\phi + \delta)}{\sqrt{1 - T_0 \sin^2[(\phi + \delta)/2]}} \end{aligned} \tag{3.35}$$

The CPR (3.35) is 2π-periodic in ϕ and vanishes (reappears) at the boundaries between ground states with opposite fermion parity. These boundaries coincides with the formation points of MBSs. In fact, we have seen that Majoranas are zero energy modes in sec 3.3. In the case considered, we can have zero energy just for $E_- = 0$. This implies

$$\tilde{\Delta}(\phi) = \alpha \tag{3.36}$$

This corresponds to a pair of Majorana fermions that can be represented via the operator $\xi_1 = -i(\eta_- - \eta_-^\dagger)$ and $\xi_2 = \eta_- + \eta_-^\dagger$. To avoid recombination, the MFs

have to be spatially separated. Looking at the actual form of the ξ_i operators

$$\xi_1 = -\frac{i}{2}\left[\left(1-e^{-i\theta}\right)d_1 + \left(1-e^{-i\theta}\right)d_2 + \left(-1-e^{i\theta}\right)d_1^\dagger + \left(-1+e^{i\theta}\right)d_2^\dagger\right] \tag{3.37}$$

$$\xi_2 = \frac{1}{2}\left[\left(1-e^{-i\theta}\right)d_1 + \left(1+e^{-i\theta}\right)d_2 + \left(1-e^{i\theta}\right)d_1^\dagger + \left(1+e^{i\theta}\right)d_2^\dagger\right] \tag{3.38}$$

Imposing the spatial separation (i.e. a Majorana fermion in one dot and the second in the other), we find a condition for θ

$$\theta = 0 \begin{cases} \xi_1 = -i[d_1 - d_1^\dagger] \\ \xi_2 = d_2 + d_2^\dagger \end{cases} \tag{3.39}$$

$$\theta = \pi \begin{cases} \xi_1 = -i[d_2 - d_2^\dagger] \\ \xi_2 = d_1 + d_1^\dagger \end{cases} \tag{3.40}$$

Thus, we finally have the condition

$$\theta(\phi) = 0 \bmod \pi \tag{3.41}$$

From eq. (3.15), we see there are two possibilities to satisfy this condition:

1. Choose equal hybridization strength $\gamma_L = \gamma_R = \gamma$. Then, $T_0 = 1$, thus $\tilde{\Delta} = \gamma|\cos[(\phi+\delta)/2] = \alpha$
2. If $\gamma_L \neq \gamma_R$, we may adjust $\phi = -\delta \pmod{2\pi}$and then we hav a MBS pair when $\gamma = \alpha$

4 Non-equilibrium case

4.1 Keldysh formalism for out of equilibrium systems

It is known that, in an equilibrium situation, the time evolution operator $\mathbf{U}(t, t')$ is such that $\mathbf{U}(-\infty, t) = \mathbf{U}(\infty, t)$, as the system recovers to the same non-perturbed state $|\phi_0\rangle$ for $t \to \pm\infty$. This fact is used while studying the perturbation theory for the Green's function, and leads to the well known Feynman diagram and Dyson's equation. In the case of a non-equilibrium situation this is not true anymore, as nothing assures that at $t = +\infty$ we will retrieve the same state we had at $t = -\infty$. In fact, with the loss of the equilibrium hypothesis, the temporal symmetry is lost too. Hence, it may seem like it is not possible to have a perturbative expansion as we had in the previous case.

The way out was given by Keldysh who redefined the time contour in order to be able to write the expectation value of an operator as a (Keldysh) time ordered expectation value. Before introducing the Keldysh formalism, it is useful to review the well known formulas of the equilibrium case:

$$\langle A(t)\rangle = \frac{\langle \Psi_I(t)|\, \mathbf{A}_I(t)\, |\Psi_I(t)\rangle}{\langle \Psi_I(t)|\Psi_I(t)\rangle} \tag{4.1}$$

Where the"I" subscript stands for Interaction (or Dirac) picture. In the adiabatic hypothesis, we can substitute $\mathbf{V}(t) \to \lim_{\eta\to 0} \mathbf{V}(t)e^{-\eta|t|}$. Assuming that at $t = -\infty$ the system was in the state $|\phi_0\rangle$ and that, at t, it has evolved to $|\Psi_I(t)\rangle$, we can write for (4.1):

$$\langle A(t)\rangle = \frac{\langle \phi_0|\, \mathbf{U}(-\infty, t)\mathbf{A}_I(t)\mathbf{U}(t, -\infty)\, |\phi_0\rangle}{\langle \phi_0|\, \mathbf{U}(-\infty, t)\mathbf{U}(t, -\infty)\, |\phi_0\rangle} \tag{4.2}$$

So, in the equilibrium case;

$$\langle A(t)\rangle = \frac{\langle \phi_0|\, \mathbf{U}(\infty, t)\mathbf{A}_I(t)\mathbf{U}(t, -\infty)\, |\phi_0\rangle}{\langle \phi_0|\, \mathbf{U}(\infty, t)\mathbf{U}(t, -\infty)\, |\phi_0\rangle}$$

And it follows

$$\langle A(t)\rangle = \frac{\langle \phi_0|\, \mathbf{T}[\mathbf{A}_I(t)\mathbf{U}(\infty, -\infty)]\, |\phi_0\rangle}{\langle \phi_0|\, \mathbf{U}(\infty, -\infty)\, |\phi_0\rangle} \tag{4.3}$$

While equation (4.2) is valid in any case the last two (4.1), (4.3) are not. In order to generalize this writing for the non-equilibrium case, we here introduce the Keldysh contour

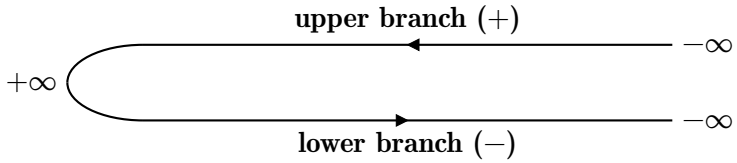

Figure 4.1: Keldish time contour

With this time contour, the system starts form the state $|\phi_0\rangle$ at $t = -\infty$, evolves out of equilibrium while the time becomes arbitrarily large to reach $t = +\infty$, then "subsequently" goes back to the initial state as the time returns to $t = -\infty$, as shown in figure 4.1. In this manner, we have recovered the temporal symmetry we had in the equilibrium case.

It is important to note that the distinction between the two branches becomes essential when we are time-ordering the operators. We define the Keldysh contour time-ordering operator $\mathbf{T}_c$ and the evolution operator along the Keldysh contour $\mathbf{U}_c = \mathbf{U}_-(-\infty, \infty)\mathbf{U}_+(\infty, -\infty)$. Then, we can write:

$$\langle A(t)\rangle = \frac{\langle\phi_0|\,\mathbf{T}_c[\mathbf{A}_I(t)\mathbf{U}_c(\infty,-\infty)]\,|\phi_0\rangle}{\langle\phi_0|\,\mathbf{U}_c(\infty,-\infty)\,|\phi_0\rangle} \tag{4.4}$$

In analogy with the known perturbative expansion for $\mathbf{U}(t, t')$, we write:

$$\mathbf{U}_+(+\infty,-\infty) = 1 + \sum_n \frac{(-i)^n}{n!}\int_{-\infty}^{+\infty} dt_1 \ldots \int_{-\infty}^{+\infty} dt_n \mathbf{T}[\mathbf{V}_I(t_1)\ldots\mathbf{V}_I(t_n)] \tag{4.5a}$$

$$\mathbf{U}_-(-\infty,+\infty) = 1 + \sum_n \frac{(-i)^n}{n!}\int_{+\infty}^{-\infty} dt_1 \ldots \int_{+\infty}^{-\infty} dt_n \overline{\mathbf{T}}[\mathbf{V}_I(t_1)\ldots\mathbf{V}_I(t_n)] \tag{4.5b}$$

The operator $\overline{\mathbf{T}}$ is defined in the lower branch of the Keldysh contour and thus the times are ordered backwards. Inserting expressions (4.5) in (4.4) we have the desired perturbative expansion of $\langle A(t)\rangle$. Furthermore, the Wick's theorem is still valid.
The Green's function is modified as follows in order to have a theory formally equivalent to the equilibrium case:

$$G_{ij}(t_\alpha, t'_\beta) = -i\,\langle\Psi_h|\,\mathbf{T}_c[\mathbf{c}_{i\sigma}(t_\alpha)\mathbf{c}^\dagger_{j\sigma}(t'_\beta)]\,|\Psi_H\rangle \tag{4.6}$$

where α and β are indices taking values $+, -$ to indicate the Keldysh contour branches.

At this point, we need to distinguish between four different possibilities for the "positioning" of the two times in the Keldysh Green's function.

- $t = t_+$ and $t' = t'_+$
  Both arguments are in the upper branch, so they are time-ordered as usual and we have

$$\begin{aligned} G^{++}_{ij} &= -i\left\langle \mathbf{T}_c[\mathbf{c}_{i\sigma}(t)\mathbf{c}^\dagger_{j\sigma}(t')]\right\rangle \\ &= -i\left\langle \mathbf{T}[\mathbf{c}_{i\sigma}(t)\mathbf{c}^\dagger_{j\sigma}(t')]\right\rangle \end{aligned} \tag{4.7}$$

From equation (4.7) we see that this is the conventional casual Green's function

- $t = t_+$ and $t' = t'_-$
  We now have to be careful and observe that a time in the lower branch is intrinsically in the "future" in respect to a time in the upper branch. We have:
  $$G_{ij}^{+-}(t,t') = i\left\langle \mathbf{c}_{j\sigma}^{\dagger}(t')\mathbf{c}_{i\sigma}(t)\right\rangle \tag{4.8}$$
  This function is sometimes referred to as the Keldysh Green's function and it plays a central role in out of equilibrium systems.

- $t = t_-$ and $t' = t'_+$
  From the considerations above
  $$G_{ij}^{-+} = -i\left\langle \mathbf{c}_{i\sigma}(t)\mathbf{c}_{j\sigma}^{\dagger}(t')\right\rangle \tag{4.9}$$
  and this function is closely related to (4.8).

- $t = t_-$ and $t' = t'_-$
  Both the times are in the lower branch, so we use the time-anti-ordering operator $\overline{\mathbf{T}}$
  $$G_{ij}^{--} = -i\left\langle \overline{\mathbf{T}}[\mathbf{c}_{i\sigma}(t)\mathbf{c}_{j\sigma}^{\dagger}(t')]\right\rangle \tag{4.10}$$
  This is really similar to the usual Green's function (4.8) but with the times ordered in the reversed sense.

A concise way to express the propagator in the Keldysh space is

$$\mathbf{G} = \begin{pmatrix} G^{++} & G^{+-} \\ G^{-+} & G^{--} \end{pmatrix} \tag{4.11}$$

And this form makes clear that we have doubled our initial time space.

In the Keldysh formalism, the perturbative expansion of the propagators becomes formally equivalent to the equilibrium case, the only difference being that now we deal with 2x2 matrixes in the Keldysh space. In time space, the Dyson's equation will be

$$\mathbf{G}(t,t') = \mathbf{g}(t,t') + \int dt_1 \int dt_2\, \mathbf{g}(t,t_1)\,\mathbf{\Sigma}(t_1,t_2)\,\mathbf{G}(t_2,t') \tag{4.12}$$

Where $\mathbf{g}$ is the unperturbed Green's function and $\mathbf{\Sigma}$ is the self-energy. In a stationary situation, propagators and self-energies will depend only on time intervals and we can compute the Fourier transform and write the Dyson's equation in the frequency space:

$$\mathbf{G}(\omega) = \mathbf{g}(\omega) + \mathbf{g}(\omega)\mathbf{\Sigma}(\omega)\mathbf{G}(\omega) \tag{4.13}$$

We remark that both equation (4.12) and equation (4.13) are in Keldysh space.

It is to be noted that in the Keldysh formalism the denominator $\langle\phi_0|\,\mathbf{U}_c\,|\phi_0\rangle$ does not play any role. It is easily seen if $|\phi_0\rangle$ is normalized since, in this case we straightforward have

$$\mathbf{U}_c = \mathbf{U}(-\infty,+\infty)\mathbf{U}(+\infty,-\infty) = 1$$

An attentive reader may arise the question on how the disconnected diagrams vanishes in this formalism: they simply cancel out between themselves at every order of the perturbation, as it can be seen using the Wick's theorem.

For later purposes, it is helpful to enumerate the main properties of the Keldysh propagators:

- The four Green's function G^{++}, G^{+-}, G^{-+}, G^{--} are not indipendent. They verify
$$\mathbf{G}^{++} + \mathbf{G}^{--} = \mathbf{G}^{+-} + \mathbf{G}^{-+} \tag{4.14}$$

- The Keldysh Green's functions are linearly related to the advanced and retarded Green's function G^{a} and G^{r}:
$$\mathbf{G}^{r} = \mathbf{G}^{++} - \mathbf{G}^{+-} = -\mathbf{G}^{--} + \mathbf{G}^{-+} \tag{4.15a}$$
$$\mathbf{G}^{a} = \mathbf{G}^{++} - \mathbf{G}^{-+} = -\mathbf{G}^{--} + \mathbf{G}^{+-} \tag{4.15b}$$

- For we have seen that the four Green's functions are not independent, we conclude only three of them are strictly necessary to express the 2x2 Keldysh matrix $\mathbf{G}$. Moreover, we can eliminate the $\mathbf{G}^{++}$ and $\mathbf{G}^{--}$ using the relation between Keldysh Green's functions and retarded and advanced Green's functions. A possible way to eliminate G^{++} and G^{--} is by means of a rotation in the Keldysh space that gives
$$\begin{pmatrix} G^{++} & G^{+-} \\ G^{-+} & G^{--} \end{pmatrix} \Longrightarrow \begin{pmatrix} 0 & G^{a} \\ G^{r} & G^{F} \end{pmatrix} \tag{4.16}$$
where $G^{F} = G^{+-} + G^{-+}$. This representation is usually known as *triangular representation*: we will denote the matrix propagators in this representation with $\widetilde{\mathbf{G}}$. Transforming the Dyson's equation from the Keldysh representation to the triangular representation, we have
$$\widetilde{\mathbf{G}} = \widetilde{\mathbf{g}} + \widetilde{\mathbf{g}}\widetilde{\mathbf{\Sigma}}\widetilde{\mathbf{G}} \tag{4.17}$$
Where the self-energy matrix has the form:
$$\widetilde{\mathbf{\Sigma}} = \begin{pmatrix} \Omega & \mathbf{\Sigma}^{r} \\ \mathbf{\Sigma}^{a} & 0 \end{pmatrix} \tag{4.18}$$
Where $\mathbf{\Omega} = \mathbf{\Sigma}^{+-} + \mathbf{\Sigma}^{-+}$. For the self-energy, we have the following relations:
$$\mathbf{\Sigma}^{r} = \mathbf{\Sigma}^{++} + \mathbf{\Sigma}^{+-} = -(\mathbf{\Sigma}^{--} + \mathbf{\Sigma}^{-+}) \tag{4.19a}$$
$$\mathbf{\Sigma}^{a} = \mathbf{\Sigma}^{++} + \mathbf{\Sigma}^{-+} = -(\mathbf{\Sigma}^{--} + \mathbf{\Sigma}^{+-}) \tag{4.19b}$$
From equations (4.17) and (4.18) we conclude that both the retarded and the advanced Green's functions satisfy their own equations
$$\mathbf{G}^{r,a} = \mathbf{g}^{r,a} + \mathbf{g}^{r,a}\Sigma^{r,a}\mathbf{G}^{r,a} \tag{4.20}$$
By similar consideration, G^{F} satisfies the following Dyson's equation:
$$\mathbf{G}^{F} = \mathbf{g}^{F} + \mathbf{g}^{F}\,\mathbf{\Sigma}^{a}\,\mathbf{G}^{a} + \mathbf{g}^{r}\,\mathbf{\Sigma}^{r}\,\mathbf{G}^{F} + \mathbf{g}^{r}\,\mathbf{\Omega}\,\mathbf{G}^{a} \tag{4.21}$$

- In order to write the Dyson's equation for the Keldysh function $\mathbf{G}^{+-}$, we first point out to an important property in Keldysh space, that is: every $+-$ element of any matrixes product can be expressed in terms of exclusively retarded, advanced and $+-$ quantities in the following manner:

$$\begin{aligned}(\mathbf{ABC}\dots\mathbf{YZ})^{+-} = \quad & \mathbf{A}^{+-}\mathbf{B}^{a}\dots\mathbf{Z}^{a} + \mathbf{A}^{r}\mathbf{B}^{+-}\mathbf{C}^{a}\dots\mathbf{Z}^{a} + \dots \\ & + \mathbf{A}^{r}\mathbf{B}^{r}\dots\mathbf{Y}^{+-}\mathbf{Z}^{a} + \mathbf{A}^{r}\dots\mathbf{Y}^{r}\mathbf{Z}^{+-} \end{aligned} \tag{4.22}$$

  We now may use this to rewrite the Dyson's equation for the standard Keldysh representation

$$\mathbf{G}^{+-} = \mathbf{g}^{+-} + (\mathbf{g}\,\mathbf{\Sigma}\,\mathbf{G})^{+-} \tag{4.23}$$

  Using (4.22) we have

$$\mathbf{G}^{+-} = \mathbf{g}^{+-} + \mathbf{g}^{+-}\,\mathbf{\Sigma}^{a}\,\mathbf{G}^{a} + \mathbf{g}^{r}\,\mathbf{\Sigma}^{+-}\,\mathbf{G}^{a} + \mathbf{g}^{r}\,\Sigma^{r}\,\mathbf{G}^{+-} \tag{4.24}$$

  The function $\mathbf{G}^{-+}$ satisfies a similar equation with $+$ and $-$ exchanged. We now want to write (4.24) in a more symmetrical form. First, we take out $\mathbf{G}^{+-}$ as common factor

$$\mathbf{G}^{+-} = (\mathbb{I} - \mathbf{g}^{r}\,\mathbf{\Sigma}^{r})^{-1}\mathbf{g}^{+-}(\mathbb{I} + \mathbf{\Sigma}^{a}\mathbf{G}^{a}) + (\mathbb{I} - \mathbf{g}^{r}\,\mathbf{\Sigma}^{r})^{-1}\mathbf{g}^{r}\mathbf{\Sigma}^{+-}\mathbf{G}^{a} \tag{4.25}$$

  From the Dyson's equation for the retarded Green function, we have

$$\mathbf{G}^{r} = \mathbf{g}^{r} + \mathbf{g}^{r}\,\mathbf{\Sigma}^{r}\,\mathbf{G}^{r} \Rightarrow (\mathbb{I} - \mathbf{g}^{r}\,\mathbf{\Sigma}^{r})\mathbf{G}^{r} = \mathbf{g}^{r} \Rightarrow \mathbf{G}^{r} = (\mathbb{I} - \mathbf{g}^{r}\,\mathbf{\Sigma}^{r})^{-1}\mathbf{g}^{r} \tag{4.26}$$

  Moreover

$$\begin{aligned}(\mathbb{I} + \mathbf{G}^{r}\,\mathbf{\Sigma}^{r})(\mathbb{I} - \mathbf{g}^{r}\,\mathbf{\Sigma}^{r}) &= \mathbb{I} + \mathbf{G}^{r}\,\mathbf{\Sigma}^{r} + \mathbf{g}^{r}\mathbf{\Sigma}^{r} + \mathbf{G}^{r}\,\mathbf{\Sigma}^{r}\,\mathbf{g}^{r}\,\mathbf{\Sigma}^{r} \\ &= \mathbb{I} + \mathbf{G}^{r}\,\mathbf{\Sigma}^{r} + \mathbf{g}^{r}\,\mathbf{\Sigma}^{r} + (\mathbf{G}^{r} - \mathbf{g}^{r})\Sigma^{r} = \mathbb{I} \end{aligned} \tag{4.27}$$

  Thus

$$\mathbf{G}^{+-} = (\mathbb{I} + \mathbf{G}^{r}\,\mathbf{\Sigma}^{r})\mathbf{g}^{+-}(\mathbb{I} + \Sigma^{a}\,\mathbf{G}^{a}) + \mathbf{G}^{r}\,\mathbf{\Sigma}^{+-}\,\mathbf{G}^{a} \tag{4.28}$$

  And analogous for $\mathbf{G}^{-+}$.

Before passing to the calculations for our model, let us consider a system of non-interacting electrons in equilibrium. Let $\mathbf{H}_0$ be the correspondent Hamiltonian. In this case, all unperturbed Green's functions depend exclusively on the difference of their time arguments and it is possible to obtain the Fourier transform in the frequency space. We still focus on the G^{+-}. From its definition in time space

$$G^{+-}_{ij}(t) = i\left\langle \mathbf{c}^{\dagger}_{j\sigma}(0)\mathbf{c}_{i\sigma}(t)\right\rangle$$

This function is evidently related to the electron distribution in equilibrium. Although the temperature is a parameter that does not explicitly appear in the Keldysh formalism, it can be introduced in the following way through the equilibrium Fermi distribution function. Evaluating the above expression for $t = 0$ and $i = j$

$$G^{+-}_{ii}(0) = i\,\langle \mathbf{n}_{i\sigma}\rangle = \int_{-\infty}^{+\infty}\frac{d\omega}{2\pi}G^{+-}_{ii}(\omega) \tag{4.29}$$

Where $\mathbf{n}_{i\sigma}$ is the average occupation of the one electron quantum state $(i\sigma)$. This equation states that $G^{+-}_{ii}(\omega) = 2\pi i \rho_{ii}(\omega) f(\omega)$ where $\rho_{ii}(\omega)$ is the electronic density of states projected on the state $|i\rangle$ and $f(\omega)$ is the Fermi distribution function. By means of a same argument, we have $G^{-+}_{ii}(\omega) = -2\pi i \rho_{ii}(\omega)[1-f(\omega)]$. This results indicates that irrespective of the one-electron basis, $G^{+-}(\omega) \propto f(\omega)$ and $G^{-+}(\omega) \propto [1 - f(\omega)]$. Now, using (4.14) and (4.15) we have

$$\mathbf{G}^{a}(t) - \mathbf{G}^{r}(t) = \mathbf{G}^{+-}(t) - \mathbf{G}^{-+}(t)$$

Therefore

$$\mathbf{G}^{+-}(\omega) = [\mathbf{G}^{a}(\omega) - \mathbf{G}^{r}(\omega)] f(\omega) \tag{4.30a}$$

$$\mathbf{G}^{-+}(\omega) = -[\mathbf{G}^{a}(\omega) - \mathbf{G}^{r}(\omega)][1 - f(\omega)] \tag{4.30b}$$

Equations (4.30) are still valid for a system of interacting electrons and will come handy in computing the form of the Josephson current in the next section.

4.2 Computing the current

The difference between the system we are considering here and what analyzed in the previous section is that we are now applying an external voltage within the superconductors. Hence, the system is now out of equilibrium. The definition of the left/right current, obviously, is the same as the one given above. Nevertheless, the actual computation of the Josephson current has a different form, following the Keldysh formalism introduced in the previous section. We follow the steps as in Dolcini and Dell'Anna [22].

First of all, the presence of an applied voltage can be modeled introducing a time dependence in the tunneling coupling, i.e. writing

$$t_{j,n}(t) = t_{j,n}(0) \exp(ij\omega_V t/2)$$

and we have defined

$$\omega_V = \frac{eV}{\hbar}$$

Next, we remark that the Hamiltonian matrix h can be diagonalized via a unitary transformation U

$$d_{n\sigma} = (U_\sigma)_{nj} D_m \qquad m = 1, \dots, 4 \tag{4.31}$$

Hence, we write

$$H_d = \sum_{i=1}^{4} \epsilon_i D_i^\dagger D_i \tag{4.32}$$

We have denoted with ϵ_i the eigenvalues. In our case, they have the form

$$\epsilon_{1,2} = \mp\sqrt{\alpha^2 + B^2 + \epsilon^2 - \sqrt{2}\sqrt{B^2(\alpha^2 + 2\epsilon^2 + \alpha^2\cos(2\chi))}} \tag{4.33a}$$

$$\epsilon_{3,4} = \mp\sqrt{\alpha^2 + B^2 + \epsilon^2 + \sqrt{2}\sqrt{B^2(\alpha^2 + 2\epsilon^2 + \alpha^2\cos(2\chi))}} \tag{4.33b}$$

We define $U_{\uparrow(\downarrow)}$ as a 2×4 upper (lower) submatrix of U.

Now, we introduce the block-diagonal 2×8 tunneling matrix

$$T_j = \begin{pmatrix} (t_{1,j}\, t_{2,j})U_\uparrow & 0 \\ 0 & -(t^*_{1,j}\, t^*_{2,j})U^*_\downarrow \end{pmatrix} \tag{4.34}$$

and its time dependence is given by

$$T_j(t) = \begin{pmatrix} e^{ij\omega_V t/2} & 0 \\ 0 & e^{-ij\omega_V t/2} \end{pmatrix} T_j(0) \tag{4.35}$$

We rewrite the j tunneling matrix as

$$H_{t,j} = \sum_{\mathbf{k}} \mathbf{\Psi}^\dagger_{\mathbf{k}}\, T_j(t)\, \mathbf{D} + \text{h.c.} \tag{4.36}$$

where we have denote with $\mathbf{D} = (D_1, \cdots, D_4, D_1^\dagger, \cdots, D_4^\dagger)^T$. We observe that the matrices T_j are in Nambu space. Adding the Keldysh structure to the Nambu form, we define the 4×16

$$\mathbf{T}_j = \begin{pmatrix} T_j & 0 \\ 0 & -T_j \end{pmatrix} \tag{4.37}$$

Thus, we can write the current in the form

$$I_j(t) = -2\text{Re} \sum_{\mathbf{k}} \text{Tr}_8\{(\sigma_z)_8[\mathbf{T}^\dagger_j(t)\mathbf{G}_{\mathbf{kj},0}(t,t)]^{+-}\} \tag{4.38}$$

Where $(\sigma_z)_8 = \sigma_z \otimes \mathbb{I}_4$. The Green function appearing in the current formula is the lead-dot Green function, with entries

$$iG^{\eta_1,\eta_2}_{\mathbf{kj},0}(t_1,t_2) = \langle \mathbf{\Psi}^{(\eta_1)}_{\mathbf{k},j}(t_1)\, (\mathbf{D}^\dagger)^{(\eta_2)}(t_2)\rangle \tag{4.39}$$

with η_1, η_2 indices in Keldysh space. Exploiting the Keldysh-Dyson equation

$$\mathbf{G}_{\mathbf{kj},0}(t,t) = \int_{-\infty}^{+\infty} g_{\mathbf{kj},\mathbf{kj}}(t,t')\mathbf{T}_j(t')\mathbf{G}(t',t) \tag{4.40}$$

where $g_{\mathbf{kj},\mathbf{kj}}$ is the Green function of the j lead and $\mathbf{G}$ is the Green function of the dot. Inserting (4.39) into (4.38), we have (overlooking the prefactors)

$$\begin{aligned} I_j &= \sum_{\mathbf{k}} \text{Tr}_8\{(\sigma_z)_8[\mathbf{T}^\dagger_j(t)\mathbf{G}_{\mathbf{kj},0}(t,t)]^{+-}\} \\ &= \sum_{\mathbf{k}} \text{Tr}_8\{(\sigma_z)_8[\int_{-\infty}^{+\infty} T^\dagger_j(t) g_{\mathbf{kj},\mathbf{kj}}(t,t')T_j(t')\mathbf{G}(t',t)dt']^{+-} \\ &= \int_{-\infty}^{+\infty} dt' \text{Tr}_8\{(\sigma_z)_8[\Sigma_j(t,t')\mathbf{G}(t',t)]^{+-} \end{aligned} \tag{4.41}$$

Where we have made use of the linearity property of the trace, the integral and the summation and we have defined

$$\Sigma_j(t,t') = \sum_{\mathbf{k}} \mathbf{T}^\dagger_j(t) g_{\mathbf{kj},\mathbf{kj}}(t',t)\mathbf{T}_j(t') \tag{4.42}$$

And the dot's Green function can be computed using the Keldysh-Dyson equation as

$$\begin{aligned}\mathbf{G} &= \mathbf{G}_0 + \mathbf{G}_0(\Sigma_L + \Sigma_R)G \\ \mathbf{G}_0 &= (\mathbb{I} - \mathbf{G}_0(\Sigma_L + \Sigma_R))\mathbf{G} \\ \mathbf{G} &= \left[\left([\mathbb{I} - \mathbf{G}_0(\Sigma_L + \Sigma_R)]^{-1}\mathbf{G}_0\right)^{-1}\right]^{-1} \\ &= \left[\mathbf{G}_0^{-1}[\mathbb{I} - \mathbf{G}_0(\Sigma_L + \Sigma_R)\right]^{-1} \\ &= (\mathbf{G}_0^{-1} - \Sigma_L - \Sigma_R)^{-1}\end{aligned} \tag{4.43}$$

and $\mathbf{G}_0$ describes the isolated dot.

We now introduce a discrete Fourier transform in order to write the current decomposed in its harmonic representation. We denote the discrete Fourier transform of an arbitrary two time arguments $f(t_1, t_2)$ with $f(n_1, n_2; \omega)$ and define it as

$$f(t_1, t_2) = \sum_{n,m=-\infty}^{\infty} \int_F \frac{d\omega}{2\pi} e^{-i(\omega + n\omega_V)t_1} e^{i(\omega + m\omega_v)t_2} f(n, m; \omega) \tag{4.44}$$

and F is the fundamental domain given by

$$F = \left[-\frac{\omega_V}{2}, \frac{\omega_V}{2}\right] \tag{4.45}$$

The inverse transformation reads

$$2\pi\delta(\omega_1 - \omega_2) f(n_1, n_2; \omega) = \int_{-\infty}^{+\infty} dt \int_{-\infty}^{+\infty} dt' f(t, t') e^{i(\omega_1 + n_1\omega_v)t} e^{-i(\omega_2 + n_2\omega_V)t'} \tag{4.46}$$

with the constraint $\omega_1,\, \omega_2 \in F$. If the function $f(t_1, t_2)$ depends only on the times difference, its discrete Fourier transform reads

$$f(n_1, n_2; \omega) = \delta_{n_1, n_2} \tilde{f}(\omega + n_1\omega_V) \tag{4.47}$$

Where $\tilde{f}(\omega)$ is the usual Fourier transform.

Before continuing in computing Σ_j, we take a step back and calculate the leads Green function $g_{\mathbf{k}j\mathbf{k}j}$. First, we not the leads are in equilibrium, so that

$$\sum_{\mathbf{k}} g_{\mathbf{k}j,\mathbf{k}j}(t, t') = \int_{-\infty}^{+\infty} \frac{d\omega}{2\pi} e^{-i\omega(t-t')} g_j(\omega) = g_j(t - t') \tag{4.48}$$

Denoting with $\rho(\epsilon_F)$ the density of states, we get (in Nambu space)

$$g_j^{r/a}(\omega) = \frac{\pi\rho(\epsilon_F)}{\sqrt{\Delta_p^2 - (\omega \pm i\eta)^2}}[-\omega\sigma_0 + \Delta_p\sigma_1] \tag{4.49}$$

Now, for $|\omega| < \Delta_p$ the square root is real and

$$g_j^{r/a}(\omega) = \pi\rho(\epsilon_F)\frac{-\omega\sigma_0 + \Delta_j\sigma_1}{\sqrt{\Delta_j^2 - \omega^2}} \tag{4.50}$$

We specify the (dimensionless) quasiparticle density of states

$$N_j(\omega) = \frac{\omega}{\sqrt{\omega^2 - \Delta_j^2}} \Theta(\omega^2 - \Delta_j^2) \tag{4.51}$$

where $\Theta(r)$ is the Heaviside step function. For $|\omega| > \Delta_j$ the square root is complex and we have

$$g_j^{r/a} = \mp i\pi\rho(\epsilon_f) N_j(\omega)[\sigma_0 - (\Delta_j/\omega)\sigma_1] \tag{4.52}$$

We now pass in the continuum limit using $\sum_{\mathbf{k}} \to \rho(\epsilon_F) \int_{-\infty}^{+\infty} d\epsilon_k$ and note that the terms linear in ϵ_k cancel out

$$\begin{aligned} \sum_{\mathbf{k}} g^{r/a}_{\mathbf{kj},\mathbf{kj}}(\omega) &= \sum_{\mathbf{k}} \begin{pmatrix} \omega \pm i\eta - \epsilon_{\mathbf{k}} & \Delta_j \\ \Delta_j & \omega \pm i\eta + \epsilon_k \end{pmatrix}^{-1} \\ &= \rho(\epsilon_F) \int_{-\infty}^{+\infty} \frac{d\epsilon}{\epsilon^2 + \Delta_j^2 - (\omega \pm i\eta)^2} \begin{pmatrix} -(\omega \pm i\eta) & \Delta_j \\ \Delta_j & -(\omega \pm i\eta) \end{pmatrix} \end{aligned} \tag{4.53}$$

Using (4.30) we get

$$g_j(\omega) = \pi\rho(\epsilon_F) \left[\tau_3 \frac{-\omega\Theta(\Delta_j - |\omega|)}{\sqrt{\Delta_j^2 - \omega^2}} + iN_j(\omega) \begin{pmatrix} 2f(\omega) - 1 & 2f(\omega) \\ 2f(\omega) - 2 & 2f(\omega) - 1 \end{pmatrix} \right]_K \otimes \begin{pmatrix} 1 & -\frac{\Delta_j}{\omega} \\ -\frac{\Delta_j}{\omega} & 1 \end{pmatrix}_N \tag{4.54}$$

And here we have denoted with τ_3 the z-Pauli matrix in Keldysh space.

We can now proceed and compute the transformed Σ_j.

$$\begin{aligned} \Sigma_j(n_1, n_2; \omega) &= \int_{-\infty}^{+\infty} dt \int_{-\infty}^{+\infty} dt' \Sigma_j(t, t') e^{i(\omega_1 + n_1\omega_V)t} e^{-i(\omega_2 + n_2\omega_V)t'} \\ &= \sum_{\mathbf{k}} \int_{-\infty}^{+\infty} dt \int_{-\infty}^{+\infty} dt' \mathbf{T}_j^\dagger(t) g_{\mathbf{kj},\mathbf{kj}}(t, t') \mathbf{T}_j(t') e^{i(\omega_1 + n_1\omega_V)t} e^{-i(\omega_2 + n_2\omega_V)t'} \\ &= \sum_{\mathbf{k}} \int_{-\infty}^{+\infty} dt \int_{-\infty}^{+\infty} dt' \mathbf{T}_j^\dagger(0) e^{-ij\sigma_z\omega_V t/2} g_{\mathbf{kj},\mathbf{kj}}(t, t') e^{ij\sigma_z\omega_V t'/2} \mathbf{T}_j(0) \\ &\quad e^{i(\omega_1 + n_1\omega_V)t} e^{-i(\omega_2 + n_2\omega_V)t'} \end{aligned}$$

We see that the two Keldysh tunneling matrices in the last line are time-independent. Thus, we can put them out of the integral. Moreover, we momentarily drop the summation in the following calculations.

$$\Sigma_j(n_1, n_2; \omega) = \int_{-\infty}^{+\infty} dt \int_{-\infty}^{+\infty} dt' e^{i(\omega_1 + n_1\omega_V - j\sigma_z\omega_V/2)t} g_{\mathbf{kj},\mathbf{kj}}(t, t') e^{-i(\omega_2 + n_2\omega_V - j\sigma_z\omega_V/2)t'}$$

We remember that the leads Green function has a $K \otimes N$ tensor structure and that the tunneling entries are in Nambu space. Thus, we consider the ij-entries in Nambu space for g and compute

$$\begin{pmatrix} e^{i[\omega_1+(n_1-j/2)\omega_V]t} & 0 \\ 0 & e^{i[\omega_1+(n_1+j/2)\omega_V]t} \end{pmatrix} \begin{pmatrix} g_{11} & g_{12} \\ g_{21} & g_{22} \end{pmatrix} \begin{pmatrix} e^{-i[\omega_2+(n_2-j/2)\omega_V]t'} & 0 \\ 0 & e^{-i[\omega_2+(n_2+j/2)\omega_V]t'} \end{pmatrix}$$
$$= \begin{pmatrix} e^{i[\omega_1+(n_1-j/2)\omega_V]t} g_{11} e^{-i[\omega_2+(n_2-j/2)\omega_V]t'} & e^{i[\omega_1+(n_1-j/2)\omega_V]t} g_{12} e^{-i[\omega_2+(n_2+j/2)\omega_V]t'} \\ e^{i[\omega_1+(n_1+j/2)\omega_V]t} g_{21} e^{-i[\omega_2+(n_2-j/2)\omega_V]t'} & e^{i[\omega_1+(n_1+j/2)\omega_V]t} g_{22} e^{-i[\omega_2+(n_2+j/2)\omega_V]t'} \end{pmatrix}$$

Exploiting equation (4.47), we get

$$\Sigma_j(n_1,n_2;\omega) = \mathbf{T}_j^\dagger(0) \begin{pmatrix} \delta_{n_2,n_1}\left[g_j(\omega+n_1\omega_V-\frac{j\omega_V}{2}\right]_{11} & \delta_{n_2,n_1-j}\left[g_j(\omega+n_1\omega_V-\frac{j\omega_V}{2})\right]_{12} \\ \delta_{n_2,n_1+j}\left[g_j(\omega+n_1\omega_V-\frac{j\omega_V}{2})\right]_{21} & \delta_{n_2,n_1}\left[g_j(\omega+n_1\omega_V-\frac{j\omega_V}{2})\right]_{22} \end{pmatrix} \mathbf{T}_j(0) \tag{4.55}$$

The transformed dot's Green function can then be easily calculated, as the isolated Green function is easily found to be

$$\begin{aligned} \mathbf{G}_0^{-1}(n_1,n_2;\omega) &= \delta_{n_1,n_2}\mathbf{G}_0^{-1}(\omega+n_1\omega_V) \\ \mathbf{G}_0^{-1}(\omega) &= \left[\omega\mathbb{I}_8 - \sigma_z\otimes \mathrm{diag}(\epsilon_1,\dots,\epsilon_4)\right]\tau_3 \end{aligned} \tag{4.56}$$

Having all the components, we can now perform a discrete Fourier transformation on the current (4.41). We focus on the term relative to $\Sigma_j G$

$$\begin{aligned} \int_{-\infty}^{+\infty}\Sigma_j(t,t')G(t',t) &= \int_{-\infty}^{+\infty}\Bigg[\sum_{n,m=-\infty}^{+\infty}\int_F\frac{d\omega}{2\pi}e^{-i(\omega+n\omega_V)t}e^{i(\omega+m\omega_V)t'}\Sigma_j(n,m;\omega) \\ &\qquad \sum_{n_1,m_1=-\infty}^{+\infty}\int_F\frac{d\omega'}{2\pi}e^{-i(\omega'+n_1\omega_V)t'}e^{i(\omega+m_1\omega_V)t}\mathbf{G}(n_1,m_1;\omega)\Bigg]\delta_{m,n_1} \\ &= \sum_{\substack{n,m\\n_1,m_1}}\int_F\frac{d\omega}{2\pi}\int_F d\omega'\left[\Sigma_j(n,m;\omega)\mathbf{G}(n_1,m_1;\omega')\right. \\ &\qquad \left. e^{i[(\omega'-\omega)-(n-m_1)\omega_V]t}\delta\big(\omega'-\omega-(m-n_1)\omega_V\big)\delta_{m,n_1}\right] \\ &= \sum_{\substack{n,m\\n_1,m_1}}\int_F\frac{d\omega}{2\pi}\Sigma_j(n,m;\omega)\mathbf{G}(n_1,m_1;\omega+(m-n_1)\omega_V)e^{i(m-n_1-n+m_1)\omega_V t}\delta_{m,n_1} \\ &= \sum_{\substack{n,m\\m'}}e^{im'\omega_V t}\int_F\frac{d\omega}{2\pi}\Sigma_j(n,m;\omega)\mathbf{G}(m,n+m',\omega) \end{aligned} \tag{4.57}$$

Where, in the first passage, we have inserted the δ_{m,n_1} in order to be able to perform the matrix product, in the second and third passage we have performed the integration over dt' and $d\omega'$ respectively and in the fourth passage we have defined $m_1-n=m'$. Inserting (4.57) into (4.41) we finally have

$$I_j(t) = -\frac{1}{\pi}\mathrm{Re}\sum_{m=-\infty}^{+\infty}e^{im\omega_V t}\int_F d\omega \mathrm{Tr}_8(\sigma_z)_8\left[\sum_{n_1,n_2=-\infty}^{+\infty}\Sigma_j(n_1,n_2;\omega)\mathbf{G}(n_2,n_1+m;\omega)\right]^{+-} \tag{4.58}$$

This equation is formally exact and represents the ac Josephson current. Charge conservation implies

$$I_L(t) = -I_R(t) \equiv I(t) \tag{4.59}$$

Obviously, when actually calculating the current, a cut-off on the summations has to be chosen. This has to be done as to assure the convergence of $I_{L/R}$ and fulfill (4.59).

When interested in the dc Josephson current, we take $m = 0$ and

$$I_0 = -j\frac{1}{\pi}\mathrm{Re}\int_F d\omega \mathrm{Tr}_8(\sigma_z)_8 \left[\sum_{n_1,n_2=-\infty}^{+\infty} \Sigma_j(n_1,n_2;\omega)\mathbf{G}(n_2,n_1;\omega)\right]^{+-} \tag{4.60}$$

We did not manage to actually computate the current as a function of the ratio eV/Δ. Nevertheless, this is possible and we would expect to see different peaks in the graphs caused by multiple Andreev reflections as reported in [23, 24, 22]

5 Conclusions

In this work, we considered a system made by a double quantum dot in contact with two superconducting leads and focused on the Josephson current flowing through it at equilibrium.

In particular, we studied the current-phase relation in the presence of a Rashba-like spin-orbit coupling and of a Zeeman term, in the limit of large superconducting order parameter. Changing all the parameters involved, we found different current-phase relations and corresponding sets of Andreev energy levels.

We showed that the spin-orbit term makes the profile of the Josephson current very peculiar and unusual. In the presence of spin-orbit coupling and Zeeman field, in fact, the Josephson current exhibits some discontinuities as a function of the phase difference. In a certain limit, these discontinuities can be related to the formation of the so-called Majorana bound states.

In the last part of the work, we considered the same system but driven out of equilibrium by an applied voltage, deriving an explicit expression for the current. The aim was to study the effect of spin-orbit and Zeeman field (specially in the range of parameters where the corresponding equilibrium Josephson current is discontinuous) on the current-voltage curve and, in particular, on the multiple Andreev reflection peaks, which are features expected to occur for $eV/2|\Delta| < 1$. We are still working on that and we are planning to develop a code for this purpose.

5 Bibliography

[1] L. Fu and C. L. Kane, "Superconducting proximity effect and majorana fermions at the surface of a topological insulator," *Phys. Rev. Lett.*, vol. 100, no. 9, 2008. 1

[2] N. Read and D. Green, "Paired states of fermions in two dimensions with breaking of parity and time-reversal symmetries and the fractional quantum hall effect," *Phys. Rev. B*, vol. 61, no. 15, 2000. 1

[3] K. Sengupta, I. Žutić, H.-J. Kwon, V. M. Yakovenko, and S. D. Sarma, "Midgap edge states and pairing symmetry of quasi-one-dimensional organic superconductors," *Phys. Rev. B*, vol. 63, no. 14, 2001. 1

[4] D. A. Ivanov, "Non-abelian statistics of half-quantum vortices in p -wave superconductors," *Phys. Rev. Lett.*, vol. 86, no. 2, 2001. 1, 31

[5] B. Josephson, "Possible new effects in superconductive tunneling," *Phys. Lett*, vol. 1, no. 251, 1962. 1

[6] P.W.Anderson and J. Rowell, "Probable observation of the josephson tunnel effect," *Phys. Rev. Lett.*, vol. 10, no. 230, 1963. 1

[7] P. D. Gennes, "Coupling between ferromagnets through a superconducting layer," *Phys. Lett.*, vol. 1, no. 23, 1966. 1

[8] H. Bruus and K. Flensberg, *Many-body quantum theory in condensed matter physics: An Introduction.* OUP Oxford, 2004. 3

[9] J. Kondo, "Resistance minimum in dilute magnetic alloys," *Progress of Theoretycal Physics*, vol. 32, no. 1, 1964. 3

[10] P. Anderson, "A poor man's derivation of scaling laws for the kondo problem," *J. Phys. C: Solid State Phys.*, vol. 3, no. 12, 1970. 3

[11] L. Glazman and M. Raikh, "Resonant kondo transparency of a barrier with quasilocal impurity states," *Jetp. Phys.*, vol. 47, no. 8, 1988. 3

[12] T. K. Ng and P. A. Lee, "On-site coulomb repulsion and resonant tunneling," *Phys. Rev. Lett.*, vol. 61, no. 15, 1988. 3

[13] D. Goldhaber-Gordon, J. Göres, M. A. Kastner, H. Shtrikman, D. Mahalu, and U. Meirav, "From the kondo regime to the mixed-valence regime in a single-electron transistor," *Phys. Rev. Lett.*, vol. 81, no. 23, 1998. 4

[14] S. Sasaki, S. D. Franceschi, J. M. Elzerman, N. G. van der Wiel, M. Eto, S. Tarucha, and L. P. Kouwenhoven, "Kondo effect in an integer-spin quantum dot," *Nature*, vol. 405, no. 6788, 2000. 4

[15] S. Cronenwett, T. Oosterkamp, and L. Kouwenhoven, "A tunable kondo effect in quantum dots," *Science*, vol. 281, no. 5376, 1998. 4

[16] H. Jeong, A. Chang, and M. Melloch, "The kondo effect in an artificial quantum dot molecule," *Science*, vol. 293, no. 5538, 2001. 4

[17] T. Klapwijk, G. Blonder, and M. Tinkham, "Explanation of subharmonic energy gap structure in superconducting contacts," *Physica B+C*, vol. 109-110, 1982. 11

[18] G. E. Blonder, M. Tinkham, and T. M. Klapwijk, "Transition from metallic to tunneling regimes in superconducting microconstrictions: Excess current, charge imbalance, and supercurrent conversion," *Phys. Rev. B*, vol. 25, no. 7, 1982. 11

[19] M. Leijnse and K. Flensberg, "Introduction to topological superconductivity and majorana fermions," *Semicond. Sci. Technol.*, vol. 27, no. 12, 2012. 31, 33

[20] J. Alicea, Y. Oreg, G. Refael, F. von Oppen, and M. P. A. Fisher, "Non-abelian statistics and topological quantum information processing in 1d wire networks," *Nat. Phys.*, vol. 7, no. 5, 2011.

[21] A. Brunetti, A. Zazunov, A. Kundu, and R. Egger, "Anomalous josephson current, incipient time-reversal symmetry breaking, and majorana bound states in interacting multilevel dots," *Phys. Rev. B*, vol. 88, no. 14, 2013. 33

[22] F. Dolcini and L. Dell'Anna, "Multiple andreev reflections in a quantum dot coupled to superconducting leads: Effect of spin-orbit coupling," *Phys. Rev. B*, vol. 78, no. 2, 2008. 42, 47

[23] A. L. Yeyati, J. C. Cuevas, A. López-Dávalos, and A. Martín-Rodero, "Resonant tunneling through a small quantum dot coupled to superconducting leads," *Phys. Rev. B*, vol. 55, no. 10, 1997. 47

[24] M. R. Buitelaar, W. Belzig, T. Nussbaumer, B. Babić, C. Bruder, and C. Schönenberger, "Multiple andreev reflections in a carbon nanotube quantum dot," *Phys. Rev. Lett.*, vol. 91, no. 5, 2003. 47

[25] A. Kamenev, *Field Theory of Non-Equilibrium Systems*. Cambridge University Press, 2011.

[26] M. Tinkham, *Introduction to superconductivity*. Dover Pubns, 2004.